Technical Report Number 71-009

205/03/187

N71-28508

NASA CR-119031

ELECTRON HEATING PROCESSES IN THE MIDDLE IONOSPHERE

by

Tieh Chun Chang

CASE FILE COPY

UNIVERSITY OF MARYLAND
DEPARTMENT OF PHYSICS AND ASTRONOMY
COLLEGE PARK, MARYLAND

This is a preprint of research carried out at the University of Maryland. In order to promote the active exchange of research results, individuals and groups at your institution are encouraged to send their preprints to

PREPRINT LIBRARY
DEPARTMENT OF PHYSICS AND ASTRONOMY
UNIVERSITY OF MARYLAND
COLLEGE PARK, MARYLAND
20742

U.S.A.

APPROVAL SHEET

Title of Thesis: Electron Heating Processes in the Middle Ionosphere.

Name of Candidate: Tieh Chun Chang
Doctor of Philosophy, 1970

Thesis and Abstract Approved:

Richard T. Bettinger

Richard T. Bettinger
Assistant Professor of Physics
Department of Physics and Astronomy

Date Approved: December 14, 1970

VITA

Name: Tieh Chun Chang

Permanent Address: 7015 Highview Terrace, Hyattsville, Maryland 20782

Degree and Date to be conferred: Doctor of Philosophy, 1970

Date of Birth: [redacted]

Place of Birth: [redacted]

Secondary Education: Normal University (Shih Fen Ta Hsueh) Teaching High School, Taipei, Taiwan

Collegiate Institutions Attended	Dates	Degrees	Date of Degree
Cheng Kung University Tainan, Taiwan	1960-1964	B. S.	1964
University of Maryland, College Park, Maryland	1965-1969	M. S.	1969
University of Maryland, College Park, Maryland	1969-1970	Ph.D.	1970

Major: Atmospheric Physics

Minor: Plasma Physics

Positions Held: Research Assistant, Department of Physics and Astronomy, University of Maryland, 1966 - Present

Teaching Assistant, Department of Physics and Astronomy, University of Maryland, 1965 - 1966

ABSTRACT

Title of Thesis: Electron Heating Processes in the Middle Ionosphere

Tieh Chun Chang, Doctor of Philosophy, 1970

Thesis directed by: R. T. Bettinger, Assistant Professor of Physics

In this study, the equilibrium distribution functions for electrons in the ionospheric plasma have been calculated for the energy interval of 0 - 15 ev, utilizing data collected in a pulse probe experiment carried out by Dr. Philip T. Huang on board the sounding rocket NASA 18.12 which was launched from Wallops Island, Virginia into the normal daytime ionosphere.

By using the densities and characteristic temperatures of superthermal and thermal electrons, the electron heat input rates have been calculated to be between 3×10^3 ev/cm^3-sec and 1.5×10^4 ev/cm^3-sec in the altitude range between approximately 120 and 240 km. The correlation between the electron heat input rates and the heat loss rates in this altitude range has been studied.

The equilibrium energy distributions of the secondary electrons in the middle ionosphere by solar ionizing radiation have been calculated for electrons with energies less than 15 ev. A high energy electron distribution ($E \geq 15$ ev) contributes the retarded probe current which appears to be a linear function of the retarding probe potential.

ELECTRON HEATING PROCESSES

IN THE MIDDLE IONOSPHERE

by

Tieh Chun Chang

August 1970

Dissertation submitted to the Faculty of the
Graduate School of the University
of Maryland in partial fulfillment of
the requirements for the degree of
Doctor of Philosophy
1970

ACKNOWLEDGMENTS

I would like to express my gratitude to Dr. Richard T. Bettinger for the encouragement and direction that he has given me throughout my graduate studies. I especially wish to thank Dr. Philip T. Huang for permission to use his measurements, which made this research study possible.

I also wish to extend my deepest gratitude to Dr. T. J. Rosenberg for critically reading the thesis and Dr. E. J. R. Maier for useful discussions. Helpful discussions with my colleagues, Jerome Bohse and Frank Huang are gratefully acknowledged.

Finally, I would like to thank Mrs. Virginia Levy for editing the manuscript, and Miss Betty Chih for her efficient typing of the manuscript.

Financial support for this research project was provided by National Aeronautics and Space Administration Grant NGR 21-002-057. Computer time was provided by the Computer Science Center of the University of Maryland under National Aeronautics and Space Administration Grant NSG-398.

TABLE OF CONTENTS

Chapter		Page
I.	INTRODUCTION	1
II.	THE PULSE PROBE	7
	A. The Langmuir Probes	7
	B. Gridded Probes	14
	C. Collection of Data	23
III.	THERMAL STRUCTURE OF THE MIDDLE IONOSPHERE	28
	A. Introduction	28
	B. Heat Input from Superthermal Electrons	29
	C. Cooling Processes of Electron Gas	34
	1. Cooling by Ion Gas	34
	2. Cooling by the Neutral Atmosphere	39
	D. Results and Discussion	48
IV.	THE PRODUCTION OF SUPERTHERMAL ELECTRONS	63
	A. Introduction	63
	B. Production of Photoelectrons	65
	C. Cooling Processes of Photoelectrons	69
	D. Equilibrium Energy Distribution of Superthermal Electrons	73
	E. Delta Function in the Distributions	80
	F. Results and Discussion	82
V.	SUMMARY AND CONCLUSIONS	86
	A. Summary	86
	1. Results of Calculations	86
	2. Possible Errors in the Calculations	87
	B. Conclusions	89

TABLE OF CONTENTS
(Continued)

Page

REFERENCES CITED 92

LIST OF FIGURES

Figure		Page
2.1	Ratio of Sheath Radius to Probe Radius vs. Applies Voltage	13
2.2	Nike-Tomahawk 18.12 Payload Section	20
2.3	Vehicle Potential vs. Altitude 18.12 Pulse Probe	22
2.4	Reduced Probe Current vs. Sweep Potential (18.12, Ascent)	25
2.5	Probe Current vs. Sweep Potential 233 km (18.12, Ascent) 10 R Section, DC Mode	26
3.1	Ionosonde Electron Concentration Taken at Time of Nike-Tomahawk 18.12 Launch (March 30, 1967)	31
3.2	Electron Heating Rate by Butler and Buckingham Method	36
3.3	Electron Heating Rate by Edward Desloge Method	32
3.4	Neutral Densities vs. Altitude (Normalized Hedin Model)	42
3.5	Atmospheric Temperature vs. Altitude (Dalgarno, et al., 1963)	43
3.6	Total Thermal Electron Cooling Rate	49
3.7	Thermal Electron Cooling Rate by Elastic Collision with N_2	50
3.8	Thermal Electron Cooling Rate by Elastic Collision with O_2	51
3.9	Thermal Electron Cooling Rate by Elastic Collision with O	52
3.10	Thermal Electron Cooling Rate by Excitation of Fine Structure Levels of Atomic Oxygen	53

LIST OF FIGURES
(Continued)

Figure		Page
3.11	Thermal Electron Cooling Rate by Excitation of Atomic Oxygen Metastable State	54
3.12	Thermal Electron Cooling Rate by Electron-Ion Columb Collision	55
3.13	Percentage Losses and Estimated Errors for Dominant Loss Processes	56
3.14	Thermal Electron Cooling Rate by Excitation of Vibrational State of N_2	61
4.1	Primary Photoelectron Production Rate	70
4.2	Accumulated Production Rate vs. Energy	71
4.3	Spatial Energy Loss Rate of an Energetic Electron vs. Energy	74
4.4	Neutral Energy Loss vs. Energy	75
4.5	Total Energy Loss Rate vs. Energy	76
4.6	Superthermal Electron Energy Distribution vs. Energy	78
4.7	Photoelectron Energy Distribution Function ..	79
4.8	Current due to Delta Function on Equilibrium Energy Distribution	83

CHAPTER I

Introduction

The ionosphere may be defined as the part of the earth's upper atmosphere where ions and electrons are present in quantities sufficient to affect the propagation of radio waves. It is considered to begin at an altitude of 50 km and to extend outwards into the magnetosphere. The ionosphere is commonly divided into several layers, which are caused by the processes of photoionization, ionic reactions and diffusion. The source of the ionizing mechanisms is a wide spectrum of solar X-ray and extreme ultraviolet (EUV) radiation. The spectrum consists of numerous emission lines generated in the chromosphere and corona of the sun, and varying amounts of continuum radiations.

The division of these layers is based on the observed altitude profile of the concentration of electrons as determined by radio wave propagation experiments. The various layers are identified by radio scientists through the use of the symbols D, E, F1, and F2.

The D region is commonly located between altitudes of approximately 50 and 85 km. Its primary neutral constituents are N_2 and O_2 , with traces of nitric oxide. NO^+, O_2^+ , and N_2^+ are the primary ions. In this region, the sources of

photoionization are believed to be Lyman alpha radiation and X-rays in the 1 to 8 Å wavelength interval. The relative importance of X-rays in this range, however, is doubtful because the intensity of these rays is ordinarily quite low except during times of solar disturbances. An outstanding feature of D region is the existence of a large number of negative ions, caused by electrons attaching themselves to oxygen molecules to form the negative ion O_2^-. The ratio of the negative ion density to electron density at 70 km is close to unity during the day.

The altitude range between approximately 85 km and 150 km has often been called the E region, and contains large amounts of N_2 and O_2 molecules. Above 120 km, the O_2 molecules have been dissociated to form atomic oxygen. EUV and X-rays in the approximate range 8 - 140 Å are usually considered as the major sources of ionization in this region. In addition, the photoelectrons produced by X-rays can produce secondary ionization in this layer. Monochromatic Lyman beta radiation here produces a layer of ions and electrons centered around 105 km with a noontime electron density of approximately $10^5/cm^3$. In this region, electron concentration shows a strong diurnal effect with maximum occurring shortly after noon; the ionization, however, does not entirely disappear at night. Antonova and Ivanov-Kholodnyy (1961) have suggested that this night time

ionization is due to the influx of soft electrons from the magnetosphere.

In the F region, the main neutral constituents are O and N_2 . Traces of O_2 , N, and NO are also common. The formation of this region is believed to be cuased by the extreme ultraviolet solar radiation in the wavelength range 150 to 900 Å . The two maxima of electron density in the F region are known as the F1 maximum, located around 200 km, with electron densities near $10^5/cm^3$, and the F2 maximum, found between 250 and 400 km, with electron densities near $10^6/cm^3$. In this region, the peak in electron density distribution varies with the time of day, season, solar cycle, and latitude. Although the F1 and F2 regions appear distinct, they are actually generated by the same ionizating radiation. Since the height of the F1 peak (200 km) is different from the height of maximum production of electrons by solar radiation (150 km), it indicates that the formation of the F region is more complex than the explanations gives thusfar.

The main production and loss processes in the F region can be expressed as:

Production: $$A + h\nu \longrightarrow A^+ + e \qquad (1.1)$$

$$\text{Loss:} \quad \begin{cases} A^+ + XY \longrightarrow XY^+ + A & (1.2) \\ XY^+ + e \longrightarrow X' + Y' & (1.3) \end{cases}$$

where equation (1.1) represents the photoionization of an atom, A , by the ionizing radiation $h\nu$, equation (1.2) represents a charge exchange between the positive ion of A and a molecule XY, and equation (1.3) represents a dissociative recombination process.

As the altitude increases, the effective recombination coefficient decreases, causing the electron density to increase beyond the peak of production. This may lead to the formation of a F1 peak. Also at higher altitudes the chemical equilibrium of the F region tends to become a diffusive equilibrium. This process generally results in a F2 peak of electron density, with a maximum occurring during both day and night.

Most of the structure of the ionosphere depends directly upon the density and composition of the neutral atmosphere. Below 100 km, the main constituents of the atmosphere are N_2 and O_2 , with small amounts of Ar and CO_2 . Above 100 km, atmospheric mixing processes become less important than diffusion. Diffusive equilibrium may begin

at about 120 km, causing the general character of the atmosphere to change. The density of each constituents decreases with height as given by the barometric law, can be expressed as:

$$n_i(z,t) = n_i(z_o) \frac{T(z_o)}{T(z,t)} \exp(- \int_{z_o}^{z} dz/H_i) \tag{1.4}$$

where the scale height H_i is defined as:

$$H_i = \frac{kT}{m_i g(z)} \tag{1.5}$$

n_i is the density of ith constituent with particle mass m_i at height Z and at time t, T is the temperature, k the Boltzmann constant and g(Z) is the acceleration due to gravity at height Z. Each neutral gas tends to be diffusively separated and each density decreases with increased altitude according to its mass and temperature. At higher altitude, the gas temperature rapidly increases by a large factor, causing a slower decrease in the density of neutral atmosphere.

In the bottomside inosphere, below the F2 maximum, photochemical processes strongly influence the composition of charged particles. The complex chain of events in the photoionization process during the day leads to the eventual heating of the neutral atmosphere. Due to the relatively poor thermal contact between electrons and the more massive particles, a substantial temperature difference

will exist between the massive particles and electrons.

Below 300 km, the assumption of a thermal equilibrium between ions and neutral particles is valid since at this height the ion gases are rapidly cooled by the neutral atmosphere. In this investigation, different aspects of the thermal structure of the middle ionosphere will be studied. Chapter II presents the results of rocket-borne pulse probes. In Chapter III the thermal electron heating and cooling processes are discussed. The photoelectron energy distribution function is discussed in Chapter IV. Summary of results will be presented in Chapter V.

CHAPTER II

Pluse Probe Experiments

In order to understand the thermal structure of the middle ionosphere, a number of experiments have been carried out in recent years. To date, the best opportunities to compare the theoretical understanding of the basic aspects of electron energy balance with the actual ionospheric environment have been provided by the results of rocket-borne Langmuir probes. The primary objective of these experiments was to measure the electron concentrations and energy distributions in the ionosphere.

A. The Langmuir Probes

The Langmuir probe is a collector, immersed in a plasma. The current is recorded as a function of the applied voltage and this information is analyzed in terms of concentrations and temperatures of the plasma constituents. Mott-Smith and Langmuir (1926) were the first to deal extensively with the theory of probes with simple geometries including: (1) planar geometry, neglecting the edge effect; (2) cylindrical geometry, neglecting the end effect; and (3) spherical geometry. Different expressions for the probe current as a function of probe to plasma potential were derived for various particle velocity distribution.

The average speed of electrons is usually greater than that of ions. When a body or a probe is immersed in ionospheric plasma, it acquires a negative equilibrium potential. The probe repels negative ions and electrons, but attracts positive ions, and thus becomes surrounded by a positive "sheath" or region of positive space charges. The total positive charge is the sheath equals the negative charge on the probe. In their derivation, Mott-Smith and Langmuir avoided the electrostatic problem by assuming that the sheath surrounding the collector could be approximated by one with a sharp outer edge, outside of which the plasma is not disturbed by the probe, and the potential is that of the undisturbed plasma. When the probe potential varies in relation to the plasma, the sheath thickness changes accordingly. Bettinger and Walker (1965) derived expressions for the sheath around the Langmuir probe for spherical and cylindrical geometry.

In the use of a cylindrical probe, if the particles have a Maxwellian velocity distribution, the current can be expressed as the following equation (Mott-Smith and Langmuir, 1926):

$$i = 2\pi R l \, I_o \, \frac{a}{R} \left\{ \left(1 - \mathrm{erf}\left(\frac{R^2 \psi}{a^2 - R^2}\right)^{\frac{1}{2}}\right) + e^{\psi} \, \mathrm{erf}\left(\frac{a^2 \psi}{a^2 - R^2}\right)^{\frac{1}{2}} \right\} \quad \psi > 0 \qquad (2.1a)$$

$$= 2\pi R l \; I_o e^{\psi} \qquad \psi < 0 \tag{2.1b}$$

where $\mathrm{erf}\,(x) = \frac{2}{\sqrt{\pi}} \int_x^{\infty} e^{-y^2}\, dy$ = complementary error function

$I_o = ne \sqrt{\frac{kT}{2\pi m}}$ = thermal current density

$\psi = \frac{eV_p}{kT}$ = nondimensional probe potential

R = the probe radius

a = the sheath radius

In the accelerating region, the current collected by the probe is a function of the sheath radius, while in the retarding region the current is independent of the sheath radius. The dimensions of the sheath surrounding a cylindrical probe with a rather large ψ are given in the following equation: (Bettinger and Walker, 1965)

$$S = \left\{ \frac{(2/3)^{\frac{1}{2}}\pi}{\ln(s/\rho)} \right\}^{\frac{1}{2}} \psi^{3/4} \tag{2.2}$$

where $S = \frac{a - R}{h}$ = nondimensional sheath thickness

$\rho = \frac{R}{h}$ = nondimensional probe radius

$h = \sqrt{\frac{kT}{4\pi ne^2}}$ = Debye length

When a probe is immersed in a plasma, the ratio of the sheath radius to the probe radius can be derived by using equation (2.2). For a plasma with a density of 10^6 electrons/cm^3 and a temperature of 2000° K, the ratio of a/R has been calculated for a different applied potential V_p .

The results are presented in Table 2.1 and plotted in Figure 2.1.

For a Maxwellian energy distribution, the electron temperature may be measured by using the i-V characteristic in the retarding region. By taking the derivative of the logarithmic current with respect to the applied voltage, equation (2.1b) can be rewritten as:

$$\frac{d \log i}{d V_p} = \frac{e}{kT} \tag{2.3}$$

A plot of log i as a function of the potential V_p will produce a straight line whose slope is inversely proportional to the temperature T. Once the electron temperature is known, the electron density can be obtained by using the equation (2.1b) together with a knowledge of the vehicle potential.

For a probe with a negative potential V_p relative to the plasma, ambient electrons with energies $E \geq eV_p$ and with proper directions of incidence may reach the probe surface and contribute to the current. The electron velocity distribution for an isotropic plasma can be found by taking the second derivative of this current with respect

TABEL 2.1

Ratio of Sheath Radius to Probe Radius as a Function of Applied Voltage

Applied Retarding Voltage (v_p)	Ratio of Sheath Radius to Probe Radius (a/R) R = h	R = 2h	R = 3h
1	5.7851	3.9008	3.3100
2	8.1754	5.2012	4.1375
3	10.1668	6.2850	4.8995
4	11.9487	7.2526	5.5760
5	13.5789	8.1413	6.1962
6	15.1054	8.9645	6.7768
7	16.5496	9.7430	7.3230
8	17.9237	10.4906	7.8449
9	19.2510	11.2049	8.3425
10	20.5270	11.8948	8.8227
11	21.7642	12.5558	9.2862
12	22.9577	13.2008	9.7344
13	24.1238	13.8286	10.1753
14	25.2618	14.4418	10.6020
15	26.3756	15.0352	11.0187

R = probe radius

h = Debye length = $\sqrt{\frac{kT}{4\pi ne^2}}$

Assume T = 2000°K and n = $10^6/cm^3$

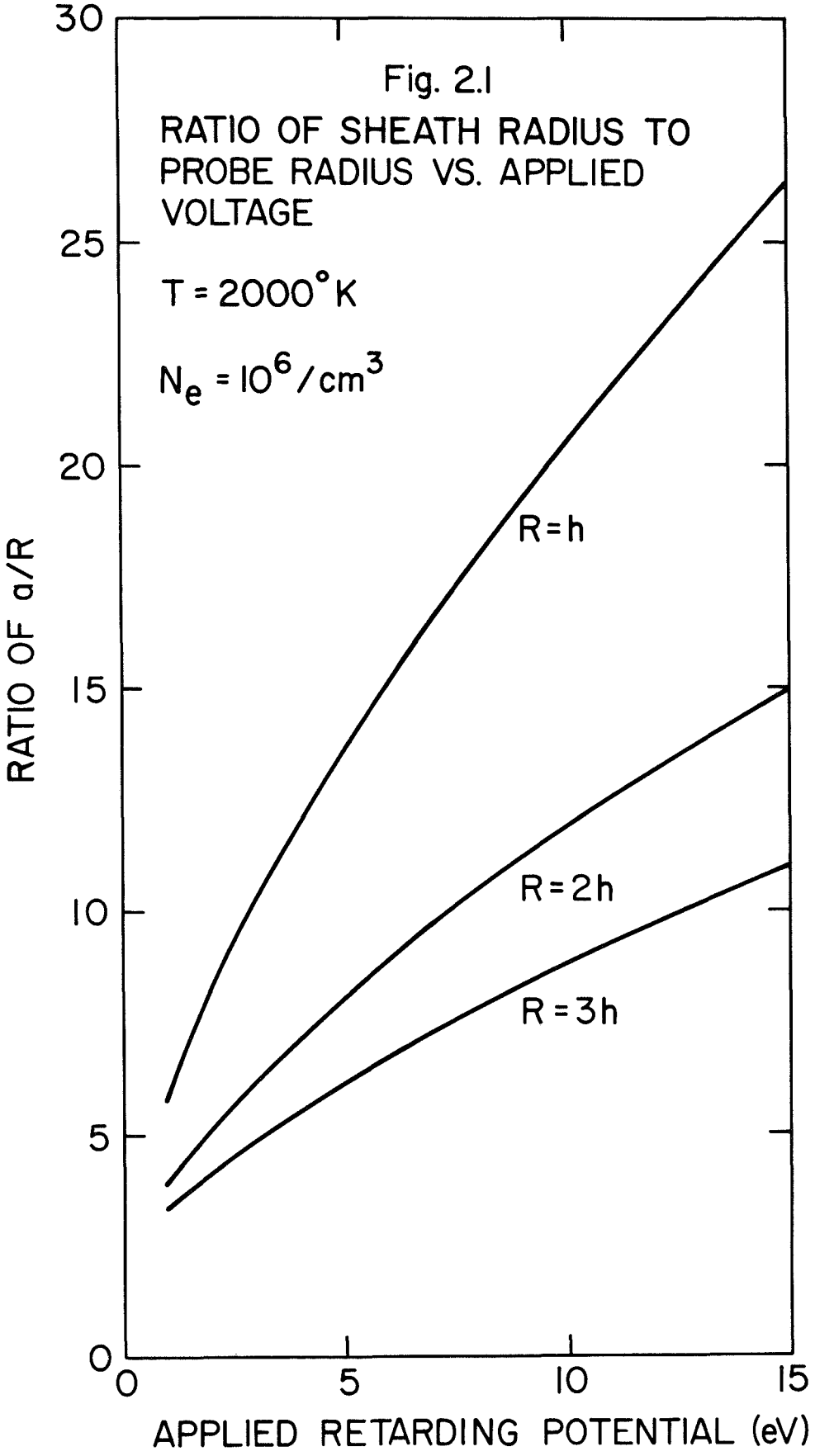
Fig. 2.1
RATIO OF SHEATH RADIUS TO PROBE RADIUS VS. APPLIED VOLTAGE
T = 2000°K
$N_e = 10^6/cm^3$
R=h
R=2h
R=3h
RATIO OF a/R
APPLIED RETARDING POTENTIAL (eV)
0
5
10
15
20
25
30

to the retarding probe potential (Druyvesteyn, 1930). For a cylindrical probe in an isotropic velocity distribution; neglecting the end effects, the Druyvesteyn relationship can be written as (Huang, 1969):

$$\frac{d^2 i}{dV_p^2} = \frac{Ae^3}{2(2meV_p)^{\frac{1}{2}}} F(eV_p) \tag{2.4}$$

where A is the total surface area of the probe, and F(E) the distribution function satisfying the normalization condition:

$$\int_0^\infty F(E)\, dE = n \tag{2.5}$$

B. Gridded Probes

One type of modified Langmuir probes are known as gridded probes, commonly referred to as "retarding potential analyzers." A number of gridded probes have been carried on various flight vehicles to determine the density and energy distribution of the ionospheric plasma (Hinteregger, 1960; Sagalyn, et al., 1963; Hanson, et al., 1964; Bettinger,

1964; Knudsen and Sharp, 1967; Harris, et al., 1967; Shea, et al., 1968; Moss and Hyman, 1968; and Huang, 1969).

Of several types of gridded probes, the main one used in experiments referred to in this paper is the pulse probe. This was first developed and tested in flight by Bettinger in 1964. It consists of an outer cage and two closely spaced grids surrounding the collector. In operation, the entire probe is immersed in a plasma and a linear potential sweep is applied to it with respect to the vehicle. The pulse probe is operated in two modes. They are: (1) DC mode, and (2) pulse mode. The chief advantage of using the pulse techniques is that the electron concentration measurements do not depend on the velocity distribution of the electrons. The pulse current I_p shows a maximum at the plasma potential and yields the ambient density without further recourse to a knowledge of the vehicle to plasma potential.

When a probe is operated in the DC mode, ambient electrons with energies $E \geq eV_p$ and the proper directions of incidence reach the surface of the collector. By letting v_ρ be the radial and v the tangential component of the velocity of an electron, with v_ρ defined to be positive when it is directed toward the origin, the total number of electrons which come to the collector in unit time may be written as:

$$i = 2\pi a\, l\, e \int_{-\infty}^{\infty} \int_{\alpha}^{\infty} v_\rho \; f(v, v_\rho)\, dv dv_\rho \tag{2.6}$$

where $f(v, v_\rho)$ is the ambient electron velocity distribution function normalized to the electron density.

$$\int_{-\infty}^{\infty} f(v, v_\rho)\, dv dv_\rho = n \tag{2.7}$$

In the equation (2.6), a is chosen as the sheath radius, such that outside the sheath the distribution is not distrubed, and α specifies the fraction of current incident on the sheath edge that actually reaches the collector, consistent with conservation of angular momentum and energy.

The laws of conservation of energy and angular momentum are reconciled in the following equation:

$$\tfrac{1}{2}m(v^2(R) + v_\rho^2\ (R)) + eV_p = \tfrac{1}{2}m\ (v^2(a) + v_\rho^2\ (a)) \tag{2.8}$$

$$v(R)R = v(a)a \tag{2.9}$$

where m is the mass of electrons and V_p denotes the retarding probe potential. By using equation (2.9), equation (2.8) may be rewritten as:

$$v_\rho^2 (R) = v_\rho^2 (a) + v^2 (a) \left(1 - \frac{a^2}{R^2}\right) - \frac{2eV_p}{m} \tag{2.10}$$

For a particle to reach the collector, the radial velocity should be at least greater or equal to zero at the probe surface, i.e., $v_\rho(R) \geq 0$, or

$$v_\rho^2 (a) \geq v^2(a) \left(\frac{a^2}{R^2} - 1\right) + \frac{2eV_p}{m} = \alpha^2 \tag{2.11}$$

For a Maxwellian velocity distribution, the total current taken by the collector for a retarding probe is

$$i = 2\pi R\ l\ n\ e\sqrt{\frac{kT}{2\pi m}}\ e^{-\frac{eV_p}{kT}} \tag{2.12}$$

When the probe is operated in the pulse mode, electrons can be accelerated toward the collector within the duration of the pulse. The electrons outside the cage near the probe are repelled away from the vicinity of the probe. The effect of the pulse on the motion of ions usually is negligible because of their relatively large inertia.

The density of the electron n inside the cage can be expressed as a linear function of the pulse current I_p

$$n = \frac{I_p}{\beta e f\ v_{eff}} \tag{2.13}$$

where v_{eff} is the effective probe volume, f is the pulse repetition rate, and β is the combined transparency of the grids surrounding the collector. The density n inside the effective volume of the probe is equal to the density immediately outside the cage surface multiplied by the transmission coefficient of the cage which is assumed to be 0.8.

The pulse probe experiments developed by Bettinger in 1964 were continued by Huang in 1969. In his investigation, Huang used a pulse probe consisting of a central collector surrounded by two closely spaced grids and an outer cage. The collector was plated with rhodium and had a diameter of approximately 0.8 in. The inner screen grids were made of stainless wires, and were located approximately 0.55 and 0.65 in., respectively, from the axis of the probe. The outer cage was supported by three insulated circular rings providing the probe with overall dimensions of 2.9 in. in height and 2.8 in. in diameter. The pulse probe was mounted on top of the payload section (Figure 2.2).

In the DC mode of operation, the two outermost elements of the probe were maintained at the same potential. A potential sweep was applied to the probe, varying from approximately plus 3 volts to minus 13 volts; the sweep rate was 54 volts/sec. The vehicle to plasma potential was approximately 2 volts throughout the flight and was obtained by the following method: first, extend the retarded thermal current which appeared as approximately a straight line on the semilog plot, towards more positive potential. Then, computing for the drift current I_o by:

$$I_o = 2\pi R l \, ne \sqrt{\frac{kT}{2\pi m}} \tag{2.14}$$

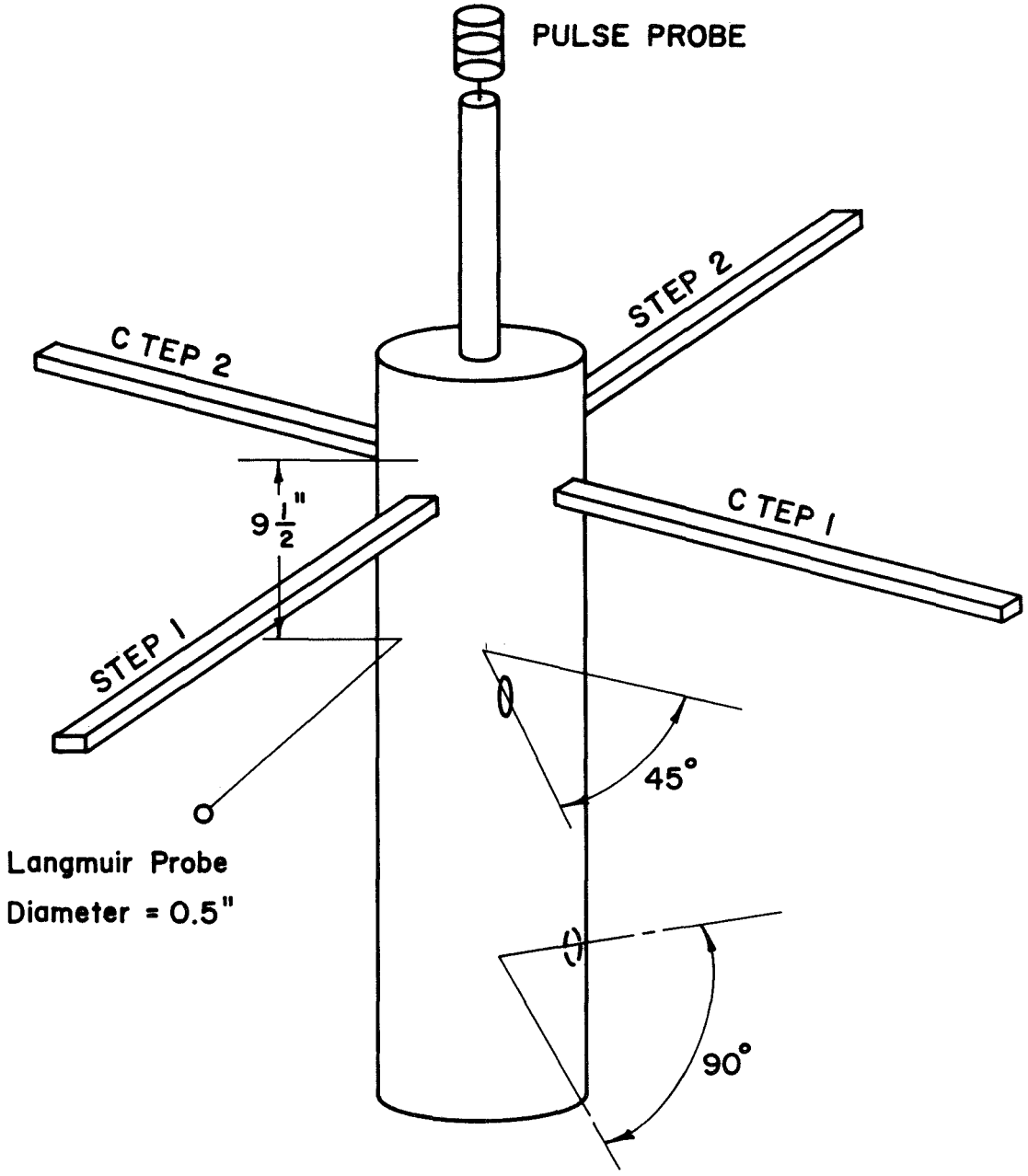

Fig. 2.2 N/T 18.12 PAYLOAD SECTION

where n is the ionosonde electron concentration. Next, locate the point on the extended current curve corresponding to I_o. The applied potential corresponding to this point was then equal to the negative vehicle potential. The values for the vehicle potentials obtained in this manner as a function of altitude are plotted in Figure 2.3. Under this arrangement of potentials, ambient electrons with sufficient energy to surmount the potential barrier and with proper direction of incidence were collected.

In the pulse mode of operation, a negative square wave of 20 volts in amplitude was applied to the outer cage relative to the inner grid. A fast rising negative pulse was then applied to the outer cage. The pulse duration was approximately 0.2μ seconds, with a frequency of 100 KHz. When the pulse was applied to the cage, all electrons inside the probe were accelerated toward the collector. It took only 5×10^{-9} seconds for an electron, initially at rest, to travel to the collector when plus 20 volts were applied to the outer cage.

A pulse duration of 0.2μ seconds provided sufficient time for most of the electrons to reach the collector. Since electrons have high mobility, the plasma quickly reverts to a state of equilibrium, to which a new pulse may be applied. The effect of the pulse on the motion of ions, for the most part, can be considered negligible

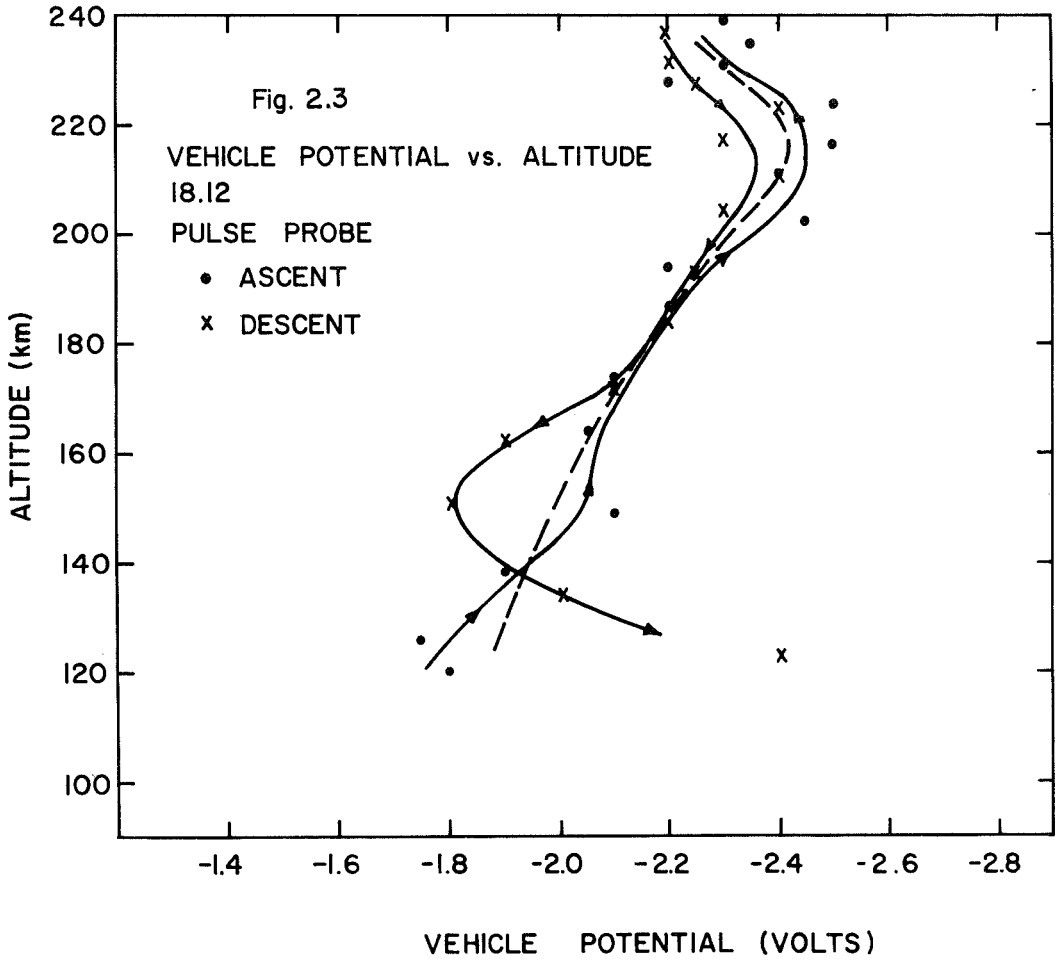
Fig. 2.3
VEHICLE POTENTIAL vs. ALTITUDE
18.12
PULSE PROBE
• ASCENT
x DESCENT
ALTITUDE (km)
240
220
200
180
160
140
120
100
-1.4
-1.6
-1.8
-2.0
-2.2
-2.4
-2.6
-2.8
VEHICLE POTENTIAL (VOLTS)

because of their relatively large inertia.

If the electron energy has a pure Maxwellian distribution, a plot consisting of log i versus applied retarding voltage will produce a straight line whose slope is proportional to the temperature. If the result is not a straight line, then the energy distribution is non-Maxwellian and can be distinguished from the results.

C. Collection of Data

In the DC mode of operation, the pulse probe current in a retarding probe potential has essentially the same current-voltage characteristic as the Langmuir probe except that there is no positive ion contribution to the total collector current. In this experiment, the collector current was monitored by a fixed range electrometer. The sensitivity of the electrometer was controlled by the value of the feedback resistor R, located between the input and the output terminals of the operational amplifier. The value at the output of operational amplifier corresponding to electrometer saturation was approximately 5.7 volts. Thus, the sensitivity range of the electrometer for a particular feedback resistence of value R ($\sim 10^5$, 10^6, 10^7, 10^8, $10^9 \Omega$), was from zero to (5.7/R) amperes. The collected current corresponding to the maximum applied retarding potential was due to the accumulation of ambient electrons with energies greater than approximately 15.5 ev. By subtracting this quantity

from the ambient electrons with energies less than $\sim$ 15 ev.

Since two distinct linear regions appeared when the current was plotted on a logarithmic scale, the current can be considered as arising from two distinct distributions, a thermal and a secondary distribution. Section AB shown in Figure 2.4 may be identified as the retarded thermal current and section BC as the retarded secondary current. The retarded thermal current produces an approximately straight line, and the majority of the electrons that contribute to this current may be characterized as a Maxwellian distribution.

The results of the secondary probe current in this experiment approximated an exponential function (usually associated with a Maxwellian distribution of energies) of the retarding probe voltage over a rather extensive portion of the curve. In the experiment the exponential slopes resulting from the secondary probe currents were about 10 times smaller than those of the exponential slopes of the thermal current section. Further expansion of the probe current is expressed in Figure 2.5 which shows a linear section between approximately 6 to 13.5 volts on the i-V plot. Since $\frac{d^2 i}{dV^2} \sim 0$ in the energy range roughly from 8 to 15 ev, it may be concluded that there exist few electrons in this range, according to the

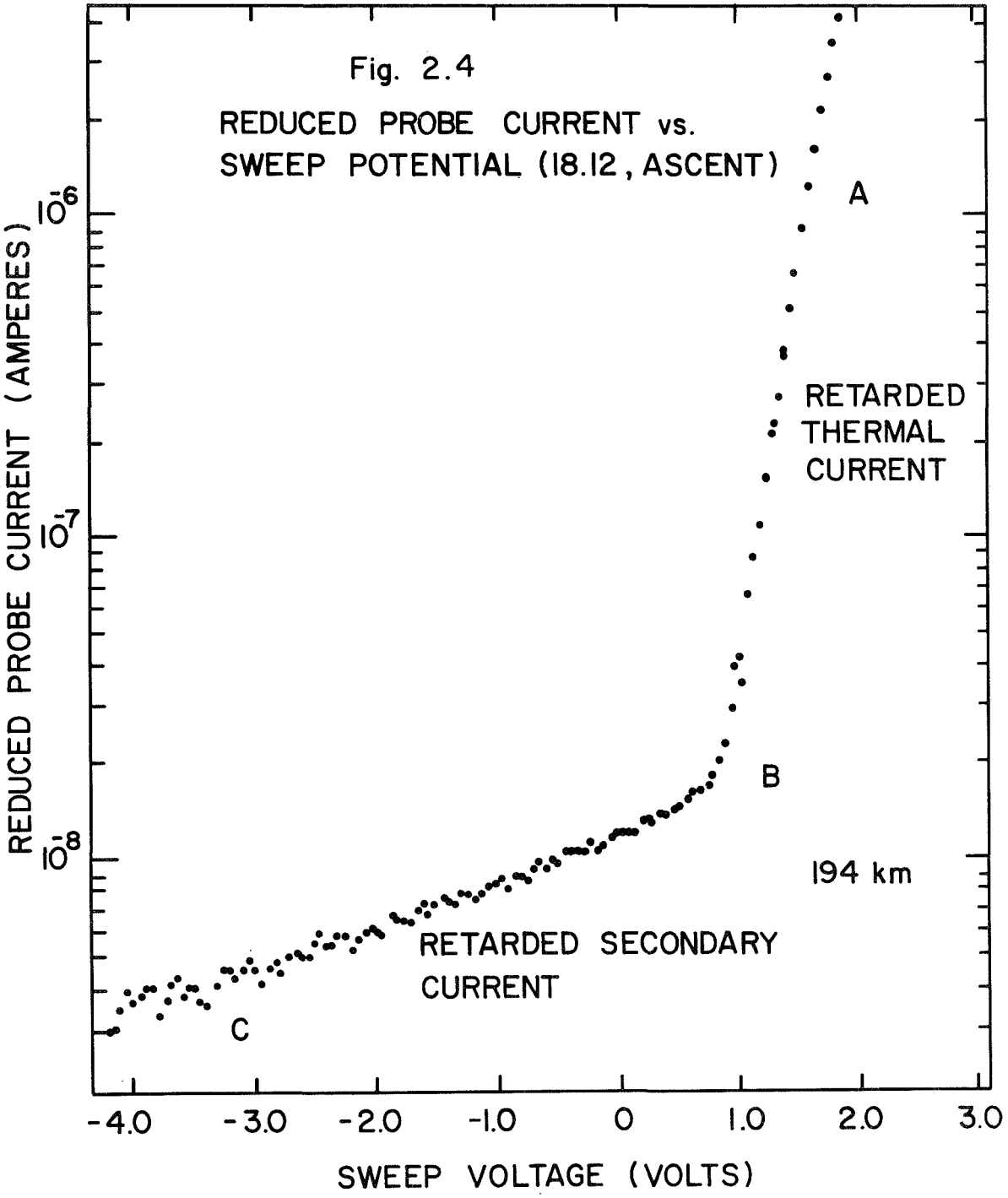
Fig. 2.4
REDUCED PROBE CURRENT vs.
SWEEP POTENTIAL (18.12, ASCENT)
A
RETARDED
THERMAL
CURRENT
B
194 km
RETARDED SECONDARY
CURRENT
C
REDUCED PROBE CURRENT (AMPERES)
10^{-6}
10^{-7}
10^{-8}
-4.0
-3.0
-2.0
-1.0
0
1.0
2.0
3.0
SWEEP VOLTAGE (VOLTS)

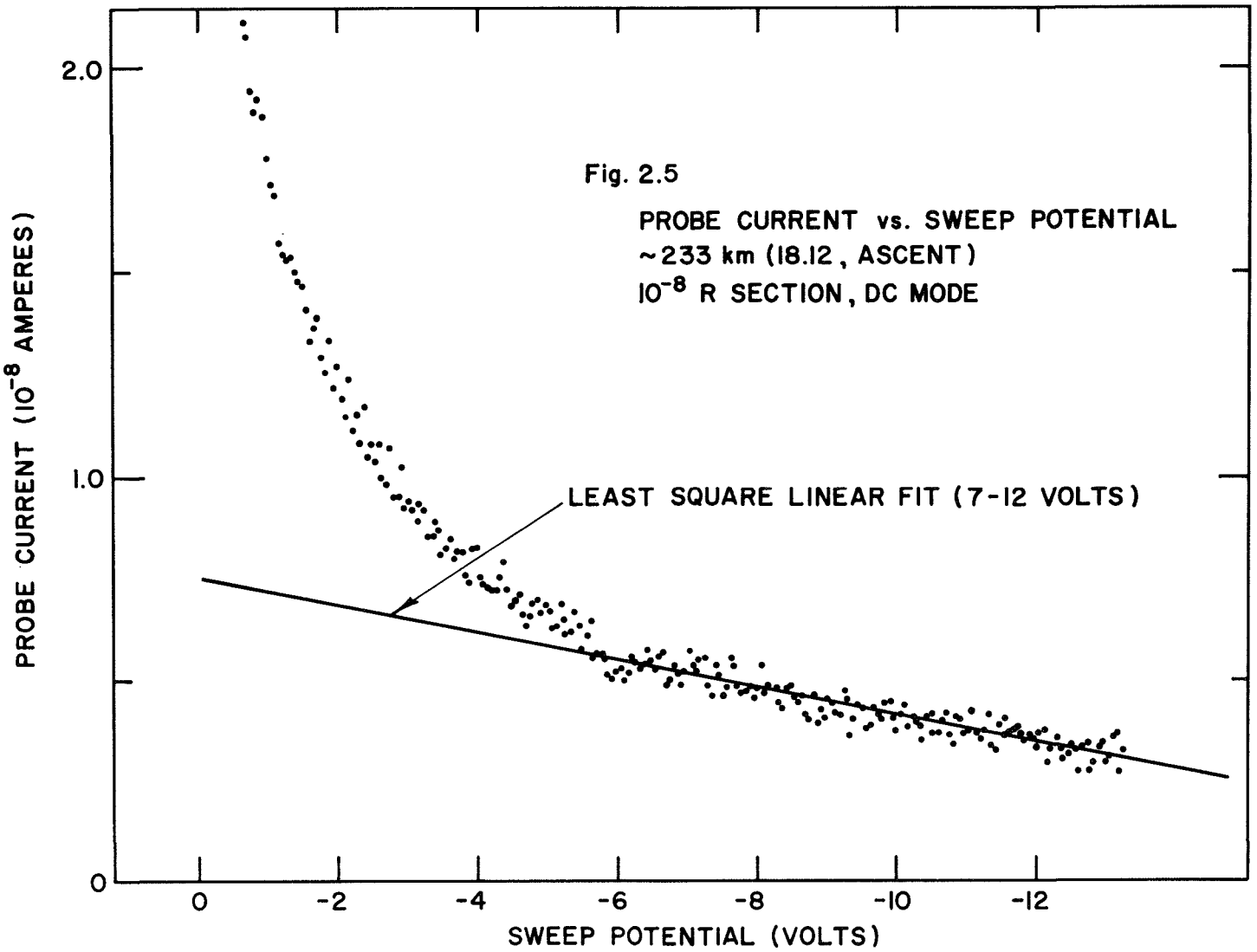
Fig. 2.5
PROBE CURRENT vs. SWEEP POTENTIAL
~233 km (18.12, ASCENT)
10^-8 R SECTION, DC MODE
LEAST SQUARE LINEAR FIT (7-12 VOLTS)
PROBE CURRENT (10^-8 AMPERES)
2.0
1.0
0
0
-2
-4
-6
-8
-10
-12
SWEEP POTENTIAL (VOLTS)

Druyvesteyn relationship. This linear current is attributed to ambient electrons with energies greater than ~ 15 ev. It is unlikely that this current is due to photoelectric or secondary emission electrons from the collector. The large positive potential bias on the collector (~ 26 ev) relative to the inner grid would suppress electron emissions from the collector significantly. Displacement currents associated with the probe sweep were less than 2×10^{-10} amperes in this experiment. The displacement current was proportional to $\frac{dV}{dt}$, the time rate of change for the sweep potential. In this experiment, $\frac{dV}{dt}$ was approximately a constant. Therefore, the overall effect of the displacement current is approximately a constant term.

In the pulse mode of operation, all electrons inside the probe are accelerated toward the collector when the pulse is on. The density of the ambient electrons in the ionosphere may be derived from the pulse current by use of equation (2.13). Unfortunately, due to failures of the probe erection mechanisms in the experiment, only a fraction of the pulse probe had proper exposure and an adequate distance from the vehicle. As a consequence, the pulse probe was limited to retarding electron energy distribution measurements.

CHAPTER III

Thermal Structure of the Middle Ionosphere

A. Introduction

Measurements made by rockets and radars confirm a deviation in the thermal equilibrium near the 120 km level and show the rapid increase of electron temperatures in comparison with the temperature of ions and neutral constituents at an altitude equivalent to that of the F2 peak. Several investigations have been carried out recently (Hanson and Johnson, 1961; Hanson, 1963; and Dalgarno, et al. 1963) to study thermal equilibrium within the middle ionosphere.

Because of the small electron-to-ion mass ratio, the amount of heat imparted to the ion gas by superthermal electrons is small compared to that imparted to the thermal electron gas. The electron-to-neutral-particle mass ratio is also very small; therefore, in the elastic collisions the energy transfer between electrons is much more efficient than the energy transfer between electrons and ions or electrons and neutral particles. This makes the temperature of the electron gas, in general, higher than that of the ion gas or of the neutral constituents in the atmosphere.

The superthermal electrons measured in this experiment may have been composed mainly of photoelectrons and secondary

electrons produced by high energy primary photoelectrons. The contribution which comes from a secondary distribution (apart from the thermal electron distribution) consists of electrons with energies ranging from approximately 1 ev to 8 ev. For these electrons, Coulomb collisions with thermal electrons and inelastic collisions with neutral constituents are the dominant mechanisms of energy loss. The loss of superthermal electrons to ions is small compared with other losses.

Hanson (1963) has indicated that up to an altitude of about 300km the photoelectron mean free path is shorter than the scale height of both the neutral and ionized components in the middle ionosphere. Hence, the rate of cooling of the superthermal electrons is assumed locally to be equal to the rate of heating at all altitudes (120 km to 240 km). The contribution of the thermal conduction flux to the heat balance in the altitude range from 120 km to 240 km has not been considered in this investigation.

The heat input rate from superthermal electrons to thermal electrons, has been calculated in Section B of this chapter. The cooling rates of thermal electrons produced by colliding with neutral constituents and encountering ions are discussed in Section C, and the results are presented in Section D.

B. Heat Input from Superthermal Electrons

In the NASA 18.12 sounding rocket flight, launched in 1967, Huang measured the temperature of superthermal electrons (electrons with energies greater than ~ 1 ev). The thermal electron temperatures were also measured in this experiment. The thermal electron densities were taken from the ionosonde electron concentration supplied by J. W. Wright of the National Bureau of Standards and are shown in Figure 3.1. Table 3.1 lists the density and temperature of both thermal electrons and superthermal electrons. At altitudes between 150 and 240 km, the measured concentration of superthermal electrons is approximately constant, $\sim 150 - 200$ electrons/cm^3, and the equivalent temperature of the secondary distribution has a range of $10{,}000^\circ K$ to $30{,}000^\circ K$.

Since the temperature of the superthermal electrons is much higher than that of the thermal electrons, it will cause them to heat the ambient electron gas by elastic Coulomb collisions. The energy loss of a charged particle in a plasma by Coulomb collisions is expressed in a formula derived by Butler and Buckingham (1962). They derived the following equation by introducing the injection of a fast charged particle into a thermal plasma:

$$\frac{dU}{dt} = - \frac{8\sqrt{\pi}\ e^4}{m\ W_t}\ F(u/W_t)\ \ln\Lambda\ n_e\ n_s\ \text{ev/cm}^3 - \text{sec} \qquad (3.1)$$

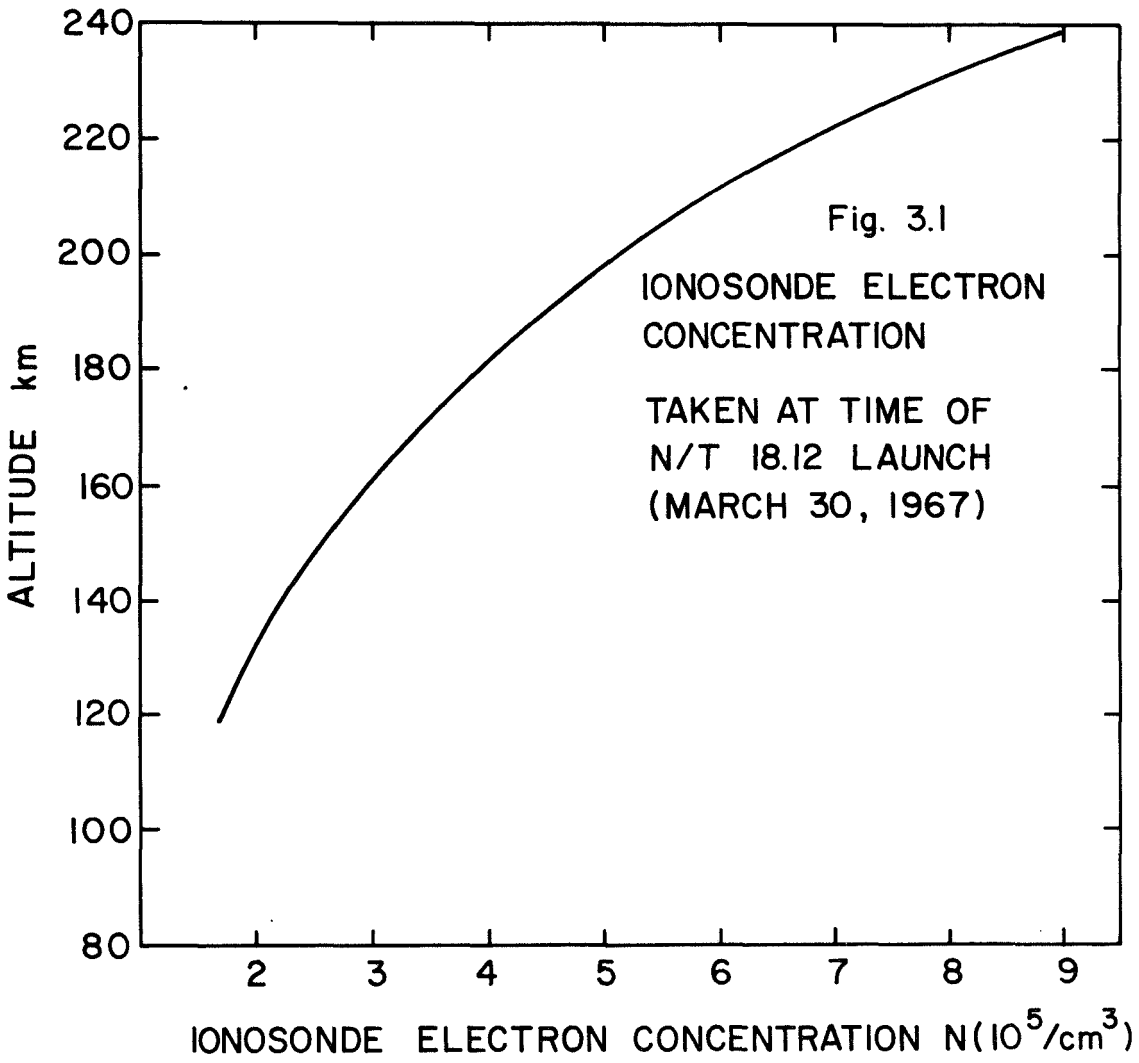
240
220
200
180
160
140
120
100
80
ALTITUDE km
2
3
4
5
6
7
8
9
IONOSONDE ELECTRON CONCENTRATION N(10^5/cm^3)
Fig. 3.1
IONOSONDE ELECTRON CONCENTRATION
TAKEN AT TIME OF N/T 18.12 LAUNCH (MARCH 30, 1967)

TABEL 3.1: CONCENTRATIONS AND TEMPERATURES OF THERMAL ELECTRONS/AND SUPERTHERMAL ELECTRONS

	Altitude (km)	n_e ($10^5/cm^3$)	T_e (^oK)	n_s ($10^2/cm^3$)	T_s (^oK)	ln Λ
Ascent	120	1.78	-----	5.8	7,980	-----
	126	1.78	1,422	8.1	8,117	15.42
	138	2.11	1,199	3.0	12,616	15.08
	149	2.57	1,390	2.4	12,508	15.20
	164	3.11	1,435	1.5	24,243	15.16
	174	3.58	1,594	1.4	23,308	15.24
	187	4.24	1,769	1.4	26,170	15.32
	194	4.75	1,978	1.6	26,767	15.43
	202	5.17	-----	1.4	31.328	-----
	211	6.01	2,239	1.4	30,553	15.49
	217	6.46	2,305	1.6	27,721	15.50
	224	7.31	2,222	1.6	25,607	15.39
	228	7.70	2,165	1.5	30,820	15.32
	231	8.13	-----	1.8	27,907	-----
	235	8.40	2,308	1.9	28,039	15.37
	237	8.80	2,338	2.1	29,261	15.37
	239	9.00	2,382	2.4	30,308	15.39
Descent	237	8.80	2,291	2.1	28,241	15.34
	231	8.13	2,136	1.6	33,074	15.27
	227	7.60	2,065	1.4	32,601	15.26
	223	7.20	2,159	1.5	32.143	15.35
	216	6.34	2,029	1.5	29,642	15.32
	210	5.85	2,123	1.4	27,170	15.43
	204	5.32	1,924	1.5	26,426	15.32
	193	4.70	1,979	1.5	31,318	15.43
	184	4.10	1,804	1.5	27,334	15.36
	171	3.50	1,757	1.5	22,484	15.40
	162	3.08	1,461	1.3	23,465	15.19
	151	2.73	1,468	1.8	19,095	15.26
	134	1.90	-----	3.6	10,050	-----
	123	1.78	-----	11.5	10,901	-----

Note: n_e is the ionosonde electron concentration recorded during the time of Nike-Tomahawk 18.12 Launch (March 30, 1967), provided by J. W. Wright of The National Bureau of Standards.

where $F(x) = \frac{1}{x}\int_{o}^{x} \exp(-x^2)dx - 2\exp(-x^2)$

and Λ is the ratio of Debye length to the distance of closest approach to the target in a head on collision (impact parameter equals to zero)

$$\Lambda = \frac{3(kT_e)^{3/2}}{(4\pi n_e)^{\frac{1}{2}}e^3}$$

W_t = thermal speed of the ambient electrons

m = mass of electron, u = speed of test particle

Another expression for the energy exchange between two Maxwellian gases at different temperatures was derived by Desloge in 1962. It can be expressed as:

$$\frac{dU}{dt} = \frac{8\, n_e\, n_s \ln\Lambda \left(1 - \frac{T_s}{T_e}\right)}{(2\pi mkT_e)^{\frac{1}{2}} \left(1 + \frac{T_s}{T_e}\right)^{3/2}} \quad \text{ev/cm}^3\ \text{sec} \qquad (3.2)$$

where T_e = Temperature of thermal electrons

T_s = Temperature of superthermal electrons

The author calculated the energy loss rate for superthermal electrons to thermal electrons through Coulomb collisions by using the above two equations. In these calculations, the approximate value of $\ln\Lambda$ was 15, and varied slowly with electron density and temperature, therefore, it was assumed to be constant. Values of calculated $\ln\Lambda$ as a function of altitude were tabulated in Table 3.1. These calculations show that Desloge's formula (3.2) constantly gives a value 30 to 40 percents higher than that derived from Butler and Buckingham's equation (3.1). The author's numerical results are listed in Table 3.2 and are depicted graphically in Figures 3.2 and 3.3.

C. Cooling Processes of Electron Gas

1. Cooling by Ion Gas

In the E and F regions the ions produced by photoionization are O^+, N_2^+, and O_2^+. The relative production rates of these ions vary with the altitude in a manner determined by the composition of the neutral atmosphere and the atmospheric absorption of specific spectral ranges of solar radiation. NO^+ can be produced by either a charge exchange or ion-atom interchange reactions. In the daytime ionosphere, NO^+ and O_2^+ are the dominant ions below 165 km. Above this altitude O^+ starts to be dominant. At night, the transition level between atomic and molecular

TABLE 3.2: ELECTRON HEATING RATES IN THE MIDDLE IONOSPHERE

	Altitude (km)	Butler and Buckingham Formula (10^3 ev/cm^3 - sec)	Desloge Formula (10^3 ev/cm^3 - sec)
Ascent	126	16.1	19.4
	138	5.8	8.4
	149	5.6	7.9
	164	3.1	4.9
	174	3.4	5.2
	187	3.8	5.9
	194	4.8	7.3
	211	4.9	7.6
	217	6.4	9.5
	224	7.5	11.1
	228	6.7	10.4
	235	9.8	14.7
	237	10.1	16.7
	239	12.7	19.3
Descent	151	3.6	5.6
	162	2.7	4.2
	171	3.6	5.4
	184	3.8	6.0
	193	4.1	6.4
	204	5.0	7.7
	210	4.9	7.4
	216	5.7	8.8
	223	6.2	9.6
	227	6.0	9.5
	231	7.3	11.5
	235	9.6	14.7
	237	11.3	17.0
	239	12.3	18.8

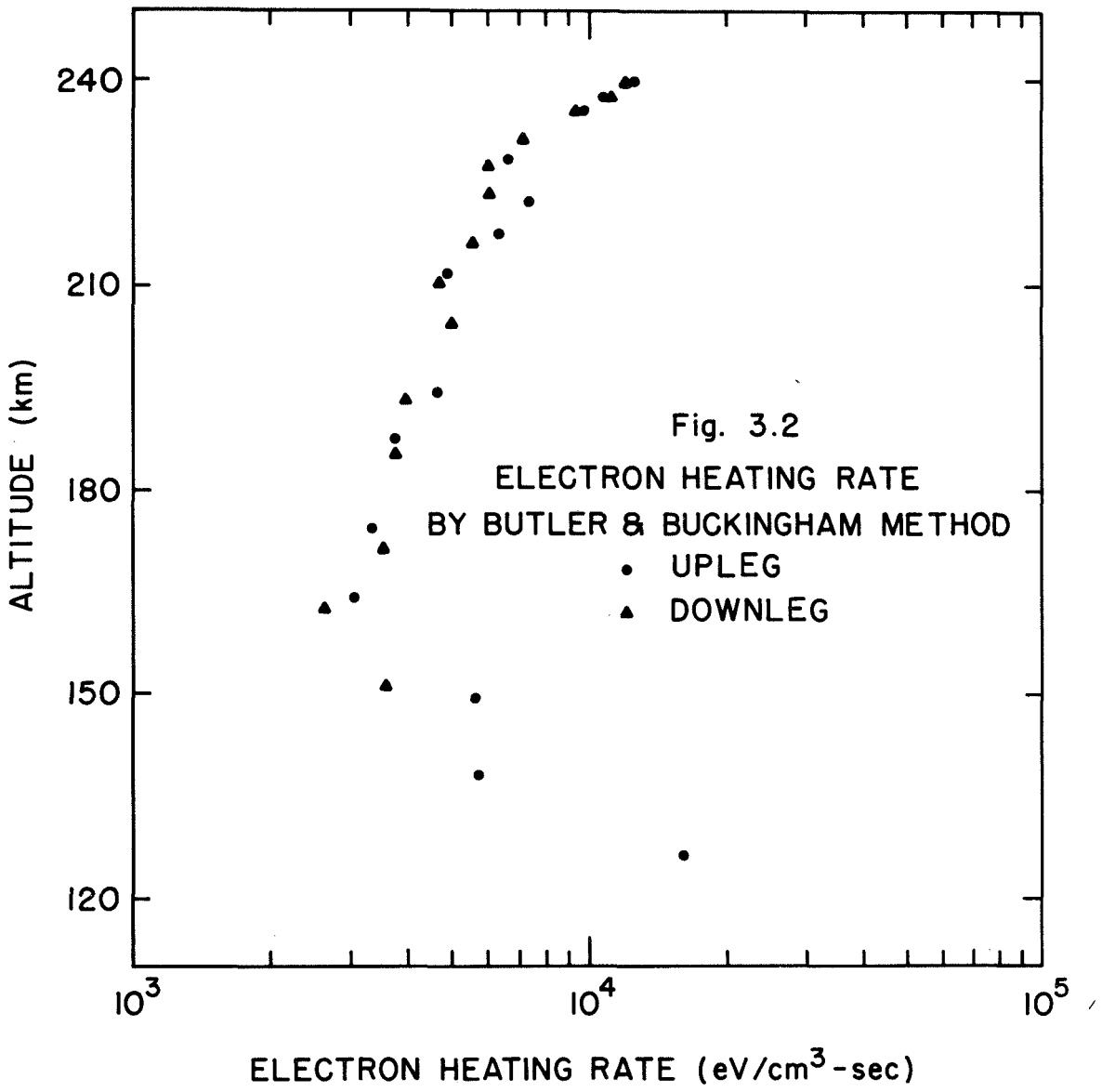
240
210
180
150
120
ALTITUDE (km)
10^3
10^4
10^5
ELECTRON HEATING RATE (eV/cm^3-sec)
Fig. 3.2
ELECTRON HEATING RATE
BY BUTLER & BUCKINGHAM METHOD
UPLEG
DOWNLEG

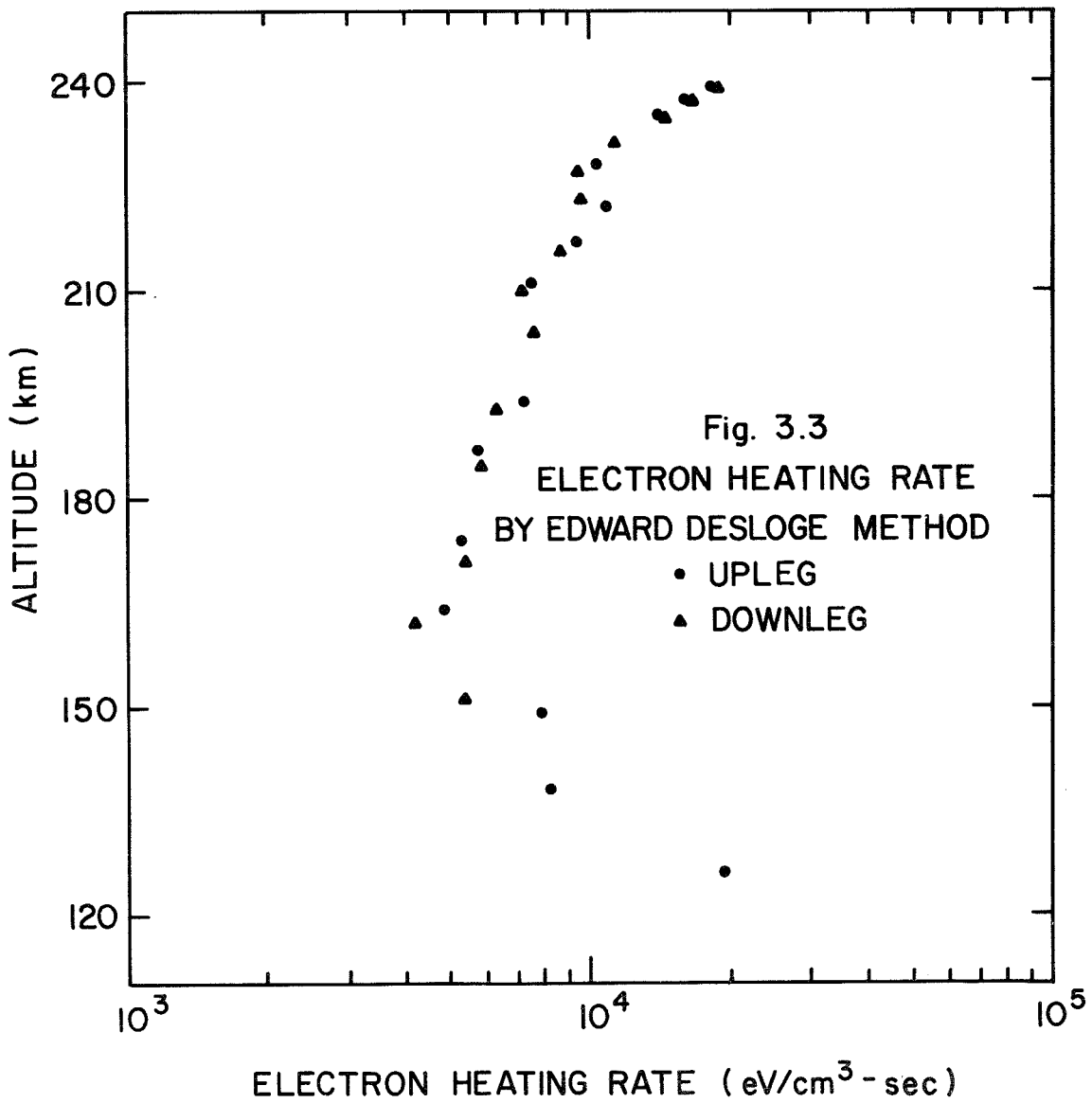
240
210
180
150
120
ALTITUDE (km)
10^3
10^4
10^5
ELECTRON HEATING RATE (eV/cm^3 - sec)
Fig. 3.3
ELECTRON HEATING RATE
BY EDWARD DESLOGE METHOD
• UPLEG
▲ DOWNLEG

ion dominance moves up to about 220 km. Other ions such as N^+, H_2O^+ are minor constituents.

Hanson and Johnson (1961) have pointed out that Coulomb collisions with positive ions play an important role in the cooling of the electron gas. The energy transfer rate between two charged gases having Maxwellian velocity distributions with different temperatures can be written as:

$$\frac{dU}{dt} = -4\sqrt{2\pi}\, n_1\, n_2 \frac{(z_1 z_2 e^2)^2}{m_1 m_2}\, k(T_1 - T_2)\, \frac{\ln\Lambda}{\left(\frac{kT_1}{m_1} + \frac{kT_2}{m_2}\right)^{3/2}} \qquad (3.3)$$

Equation (3.3) is a generalized form of equation (3.2). For single charged ions colliding with electrons, equation (3.3) is reduced to

$$\frac{dU_{e-i}}{dt} = -4\sqrt{2\pi}\, n_e\, n_i\, \frac{m_e^{\frac{1}{2}}}{m_i}\, k(T_e - T_i)\, \frac{e^4 \ln\Lambda}{(kT_e)^{3/2}} \qquad (3.4)$$

Numerically, taking $\ln\Lambda \simeq 15$, it becomes

$$\frac{dU_{e-i}}{dt} = -7.7 \times 10^6 \, n_e \, n_i \, \frac{(T_e - T_i)}{A_i \, T_e^{3/2}} \quad ev/cm^3 - sec \qquad (3.5)$$

where A_i is the ion atomic mass in amu.

By comparing the coefficient with several different experimental measurements (Banks, 1966), the energy change rate may vary by $\pm$ 10% depending upon different ionospheric conditions. In the author's calculations, it is assumed that the positive ions are mainly O^+. Under this assumption a small deviation will be introduced in the altitudes below 200 km. It is because that below 200 km the energy transfer rate is dominated by collisions with neutral particles, while above 200 km the cooling by ion gas becomes the dominating heat loss mechanism for electrons.

2. Cooling by the Neutral Atmosphere

The three primary constituents of the neutral atmosphere (O, O_2, N_2) are all effective in cooling the electron gas. The energy transfer rate $\frac{dU}{dt}$ at which unit volumes of electron gas convert their thermal energy to heat up these neutral constituents can be written as the sum of five terms:

$$\frac{dU}{dt} = \left(\frac{dU}{dt}\right)_O + \left(\frac{dU}{dt}\right)_{N_2} + \left(\frac{dU}{dt}\right)_{O_2} + \left(\frac{dU}{dt}\right)_{O_A} + \left(\frac{dU}{dt}\right)_{O_M} \qquad (3.6)$$

where the first three terms on the right hand side of equation (3.6) are the elastic collision losses, $\left(\frac{dU}{dt}\right)_{O_A}$ is the atomic oxygen fine structure loss, and $\left(\frac{dU}{dt}\right)_{O_M}$ is the atomic oxygen metastable state loss. Each of these terms is in general a function of electron temperature T_e, the neutral gas temperature T_n, and the product of the electron density n_e and the number density of each neutral constituent $\left(n(O),\ n(N_2),\ n(O_2)\right)$. The rotational loss of N_2 and O_2 is not very important above 120 km.

The model atmosphere selected for the author's calculations was based on the neutral density profiles given by Hedin and Nier (1966). The data were measured in a rocket-borne mass spectrometer experiment. The neutral densities were then normalized to the neutral density adopted by Dalgarno, et al. (1963) at 120 km. The normalization constants were 1.864, 2.234, and 2.615 respectively for molecular nitrogen, molecular oxygen, and atomic oxygen. The neutral temperature was chosen as 1000° K at the base of the exosphere, the outer fringe region of the atmosphere.

The neutral temperature and densities as a function of altitude between 120 km and 250 km are shown in Figures 3.4 and 3.5. There is still considerable uncertainty in determining the composition of the upper atmosphere. When comparing the model atmosphere adopted for this calculation and the model (S = 150) derived by Harris and Priester (1962), it can be seen that the density profile of each neutral constituent is relatively similar. The main difference between these two models arises from the different boundary conditions chosen for 120 km. These conditions are subject to change at different times of the year and at different places around the world.

Energy transfer of electrons in elastic collisions with neutral particles in the upper atmosphere has been discussed by Hanson and Johnson (1961), Hanson (1963), and Dalgarno et al. (1963). The rate at which electrons lose their thermal energy to ions and neutral gases can be determined from the results derived by Desloge in 1962. The rate of exchange of kinetic energy between electrons and ions or neutrals can be expressed as following:

$$\frac{dU_e}{dt} = -4\, n_e\, n_1 \frac{m_e}{m_1}\, k \left(\frac{8kT_e}{m_e}\right)^{\frac{1}{2}} \bar{Q}_D \left(T_e - T_1 \right) \qquad (3.7)$$

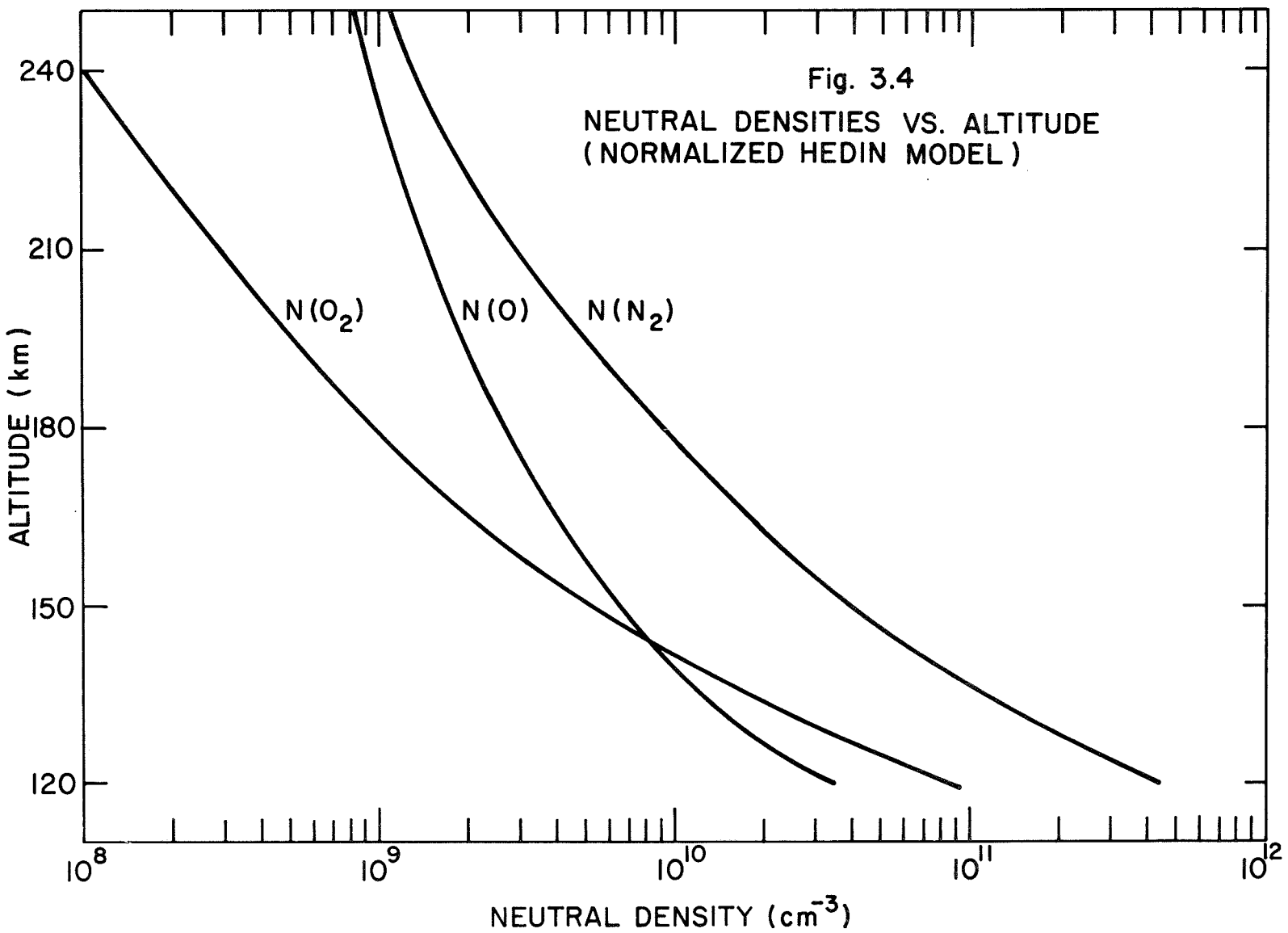
Fig. 3.4
NEUTRAL DENSITIES VS. ALTITUDE
(NORMALIZED HEDIN MODEL)
N(O2)
N(O)
N(N2)
ALTITUDE (km)
240
210
180
150
120
10^8
10^9
10^10
10^11
10^12
NEUTRAL DENSITY (cm^-3)

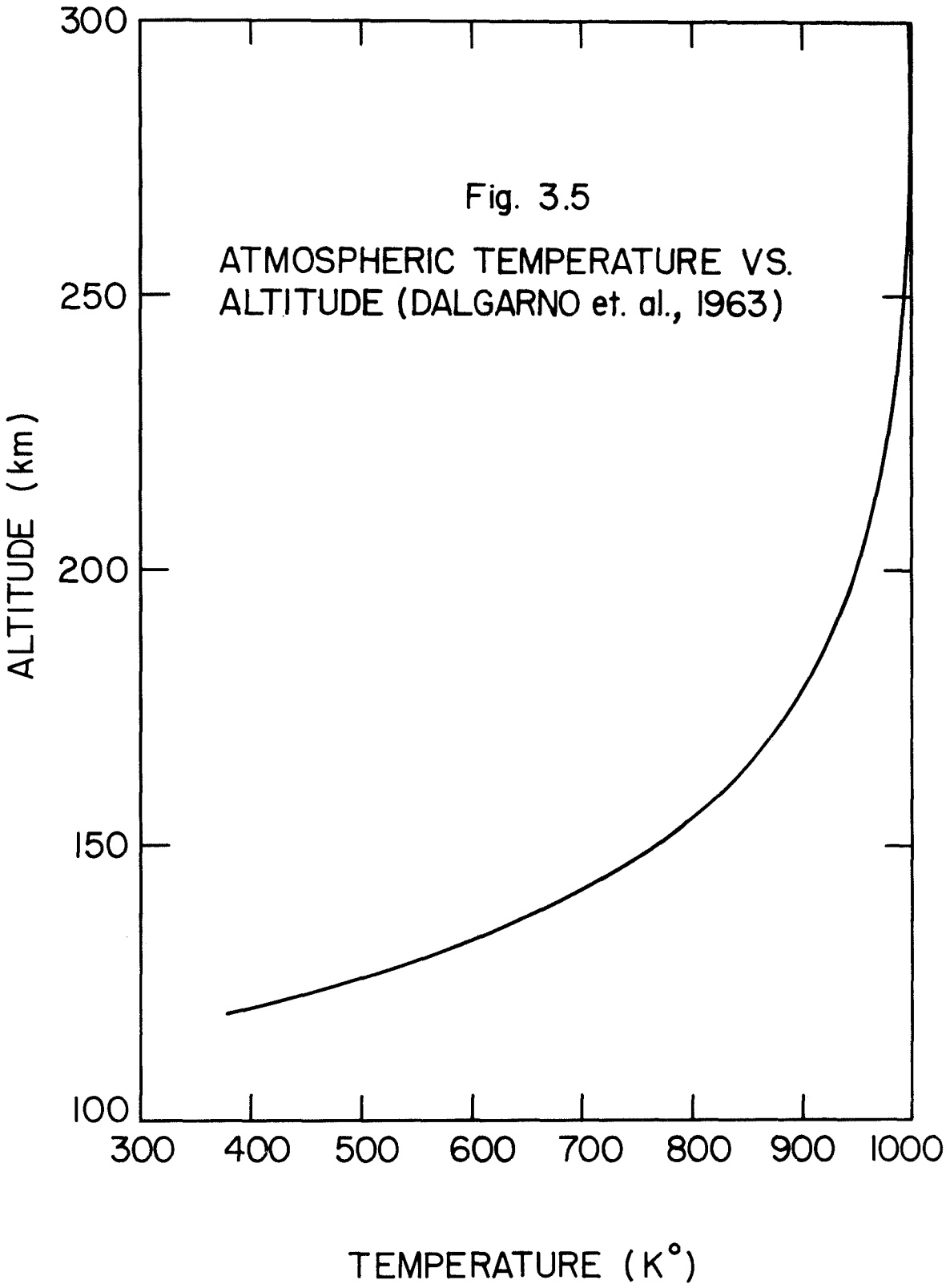
Fig. 3.5
ATMOSPHERIC TEMPERATURE VS.
ALTITUDE (DALGARNO et. al., 1963)
ALTITUDE (km)
300
250
200
150
100
300
400
500
600
700
800
900
1000
TEMPERATURE (K°)

where n_1, m_1, and T_1 are the number density, mass and the Maxwellian temperature of the ion or neutral, k is the Boltzmann constant and $\bar{Q}_D$ is the average momentum transfer cross-section, which can be expressed as:

$$\bar{Q}_D = \left(\frac{m_e}{2k\ T_e} \right) \int_0^\infty v^5\ q_D(v)\ \exp\left(- \frac{m_e v^2}{2k\ T_e}\right)\ dv \qquad (3.8)$$

where v is the electron velocity and $q_D(v)$ is the velocity dependent momentum transfer cross-section. Recently, Banks (1966) presented several energy loss rates for the individual gas components in the ionosphere derived from the available elastic cross-section data. His equation for the energy transfer rate due to molecular nitrogen was derived from the momentum transfer cross-section given by Englehardt et al. (1964), as follows:

$$\left(\frac{dU}{dt}\right)_{N_2} = -1.77 \times 10^{-19}\ n_e\ n(N_2)\ (1 - 1.21 \times 10^{-4} T_e) T_e (T_e - T_n)$$

$$ev/cm^3 - sec \qquad (3.9)$$

For the oxygen molecule, the adopted value of momentum transfer cross-section was based on Hake and Phelps's (1967) analysis,

$$\left(\frac{dU}{dt}\right)_{O_2} = 1.21 \times 10^{-18}\ n_e\ n(O_2)(1 + 3.6 \times 10^{-2}\ T_e^{\frac{1}{2}})T_e^{\frac{1}{2}}(T_e - T_n) \quad \text{ev/cm}^3 - \text{sec} \tag{3.10}$$

For atomic oxygen, there are several experimental results for the values of the total scattering cros-section, while none has been measured for the momentum transfer cross-section due to the chemical activity of oxygen atoms. Therefore the momentum transfer cross-section adopted for the atomic oxygen energy transfer rate was derived from the results of theoretical phase shift calculations which were done by Cooper and Martin (1962). The energy transfer rate can be expressed as:

$$\left(\frac{dU}{dt}\right)_{O} = -3.74 \times 10^{-18}\ n_e\ n(O)T_e^{\frac{1}{2}}\ (T_e - T_n)\ \text{ev/cm}^3 - \text{sec} \tag{3.11}$$

In a recent paper, Dalgarno and Degges (1968) have shown that an efficient way of cooling the electron gas in the E and F regions of the ionosphere is by the

excitation of the fine structure levels of atomic oxygen through inelastic collisions with thermal electrons, as in the following equation:

$$e + O(^3P_J) \longrightarrow e + O(^3P_{J'}) \tag{3.12}$$

the $^3P_0$ and $^3P_1$ levels lie 0.028 ev and 0.020 ev above the $^3P_2$ state. The importance of the heavy neutral particle analogue of equation (3.12)

$$x + O(^3P_J) \longrightarrow x + O(^3P_{J'}) \tag{3.13}$$

in the thermal balance of the neutral atmosphere has been discussed by Bates (1951).

The energy transfer rate shown below was calculated by Herman and Chandra (1969), using numerical values of the fine structure transition cross-section provided by Breig and Lin (1966).

$$\left(\frac{dU}{dt}\right)_{O_A} = -\,(3.7 - 2.92 \times 10^{-4}\, T_e)(9.06 + 6.57 \times 10^{-4} T_n) \times 10^{-13}$$

$$\times\, n_e\, n(O)\, (T_e - T_n)/\, T_n \quad \text{ev/cm}^3 - \text{sec} \tag{3.14}$$

With increasing temperatures, cooling by excitation of the metastable ^1D level of atomic oxygen (Rees, et al., 1967) becomes significant. Secondary electron excitation predominates this process up to about 250 km. The rate of this energy transfer has been derived from the excitation cross-section of Smith et al., (1967), and is shown in the following equation:

$$\left(\frac{dU}{dt}\right)_{O_M} = -1.1 \times 10^{10}\, n_e\, n(O) T_e^{\frac{1}{2}} \exp(-2.27 \times 10^4/T_e)$$

$$\Big\{ (0.406 + 0.357 \times 10^{-4}\, T_e)$$

$$- (0.333 + 0.183 \times 10^{-4}\, T_e) \times \exp(-1.37 \times 10^4/T_e)$$

$$- (0.456 + 0.174 \times 10^{-4}\, T_e) \times \exp(-2.97 \times 10^4/T_e) \Big\}$$

(3.15)

D. Results and Discussion

The calculated rates of electron cooling by neutral constituents and ions as a function of altitude are tabulated in Table 3.3. The total electron cooling rate is the sum of electron cooling rates caused by ions and neutrals. The results are shown in Figure 3.6. The energy loss rates for six individual processes are shown in Figures 3.7, 3.8, 3.9, 3.10, 3.11 and 3.12. From these tabulations, it is clear that the three dominant loss processes are: (1) excitation of fine structure levels of atomic oxygen, (2) elastic collision with N_2, and (3) electron-ion coulomb collision. The percentage losses for these three processes are plotted in Figure 3.13.

A comparison of Figures 3.4 and 3.5 with Figure 3.6 shows that the thermal electron cooling rate is approximately equal to the rate of heat input transfered from superthermal electrons to thermal electrons. This fact bears out the assumption of local heating within the altitude ranges included in these calculations.

Above 180 km, the cooling rate approximates the results of Butler and Buckingham (1962), which were derived from calculations based on test charged particles moving in a thermal plasma. Below 180 km, the cooling rate shows a closer agreement with Desloge's calculations (1962), which were derived by using two Maxwellian gases with

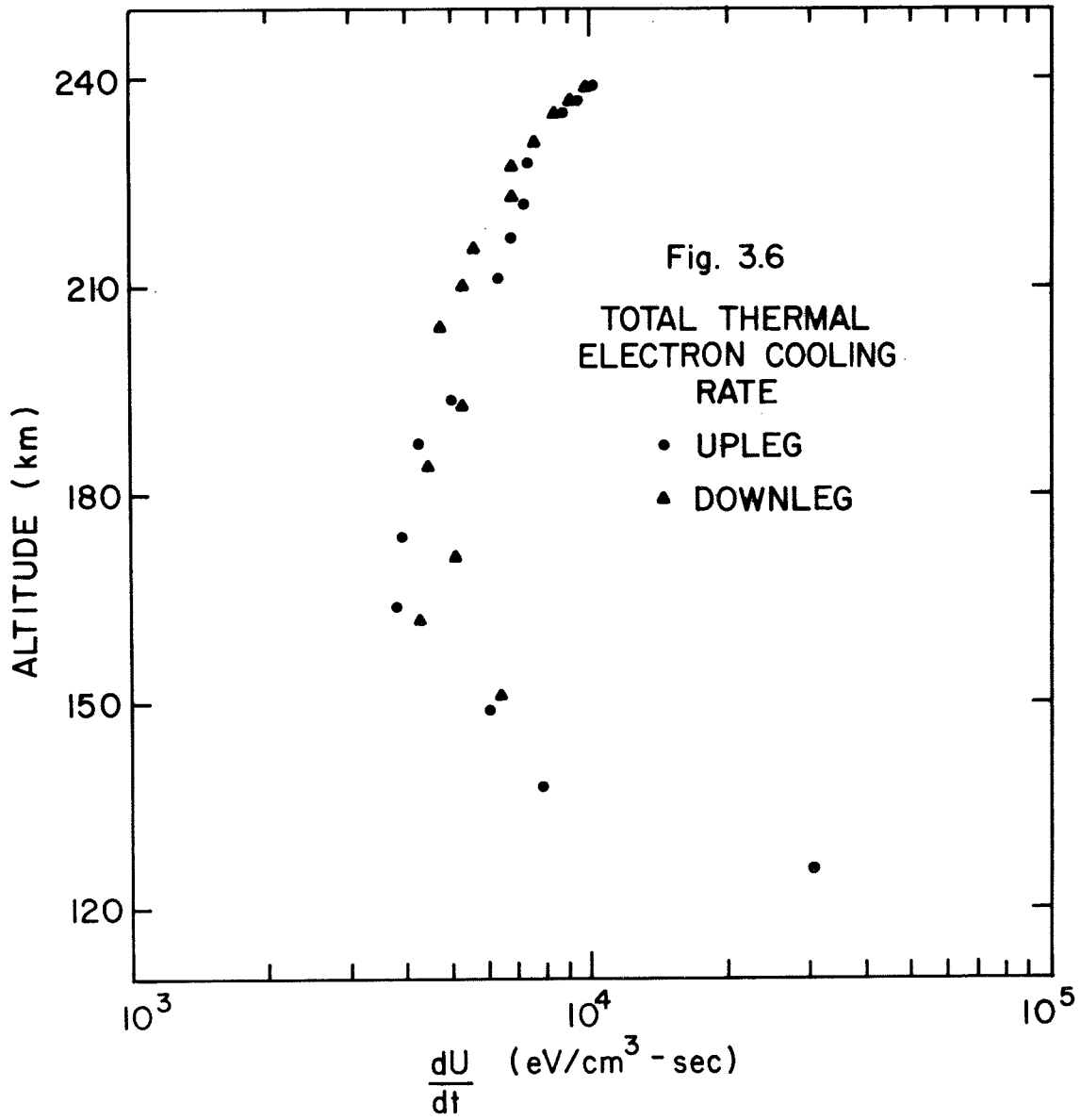
240
210
180
150
120
ALTITUDE (km)
10^3
10^4
10^5
$\frac{dU}{dt}$ (eV/cm^3 - sec)
Fig. 3.6
TOTAL THERMAL ELECTRON COOLING RATE
• UPLEG
▲ DOWNLEG

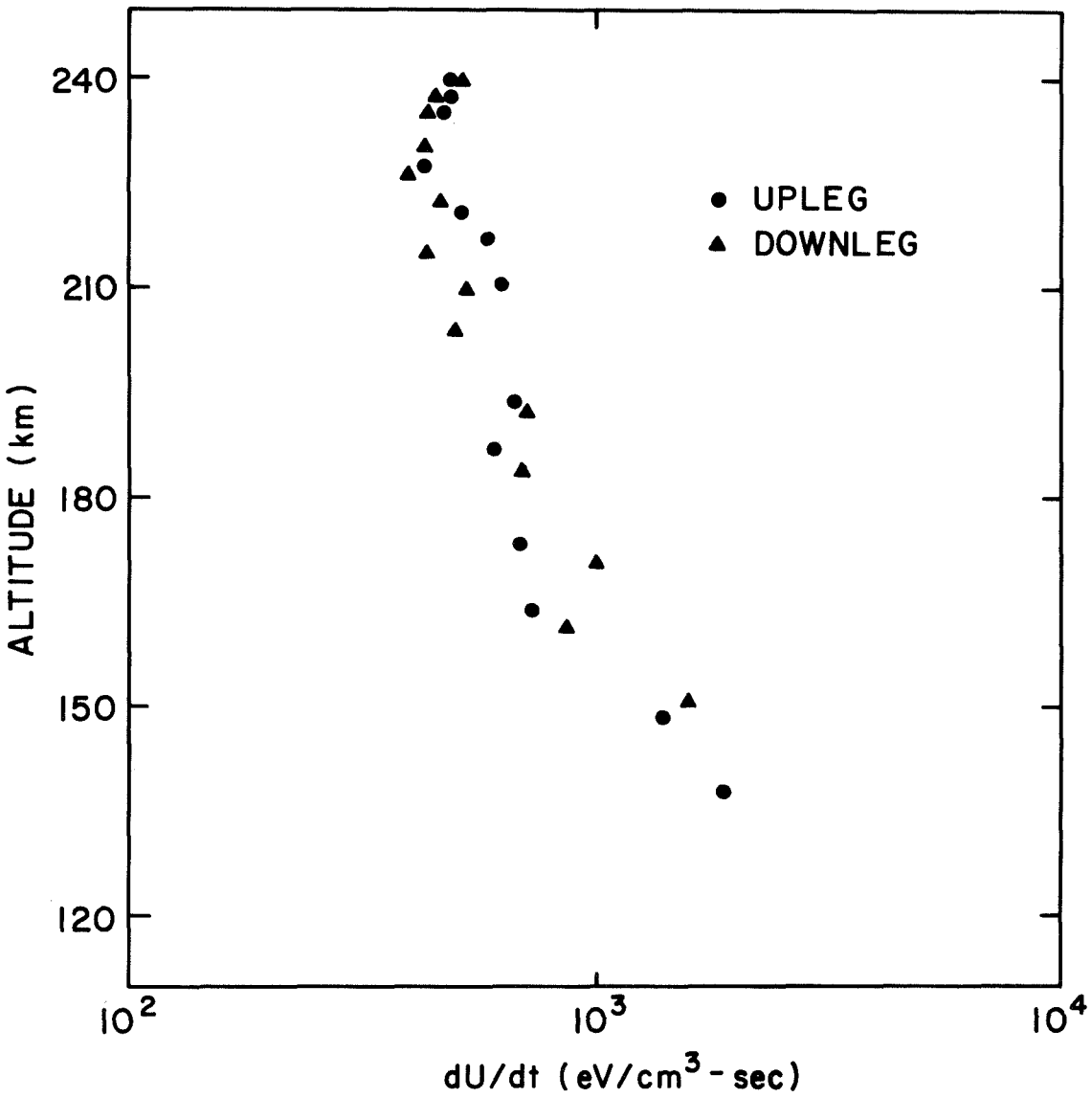

Fig. 3.7 THERMAL ELECTRON COOLING RATE BY ELASTIC COLLISION WITH N_2

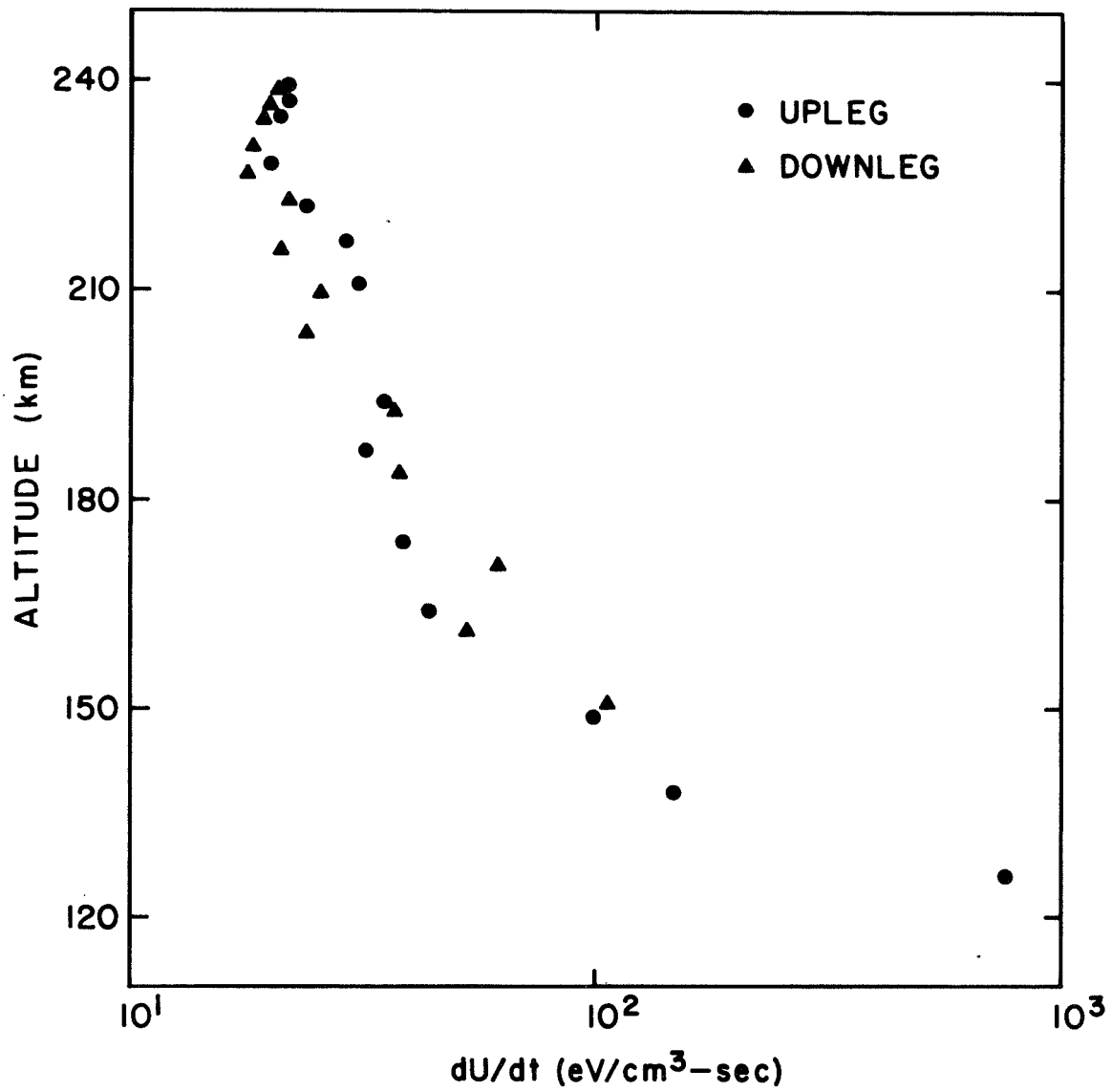

Fig. 3.8 THERMAL ELECTRON COOLING RATE BY ELASTIC COLLISION WITH O_2

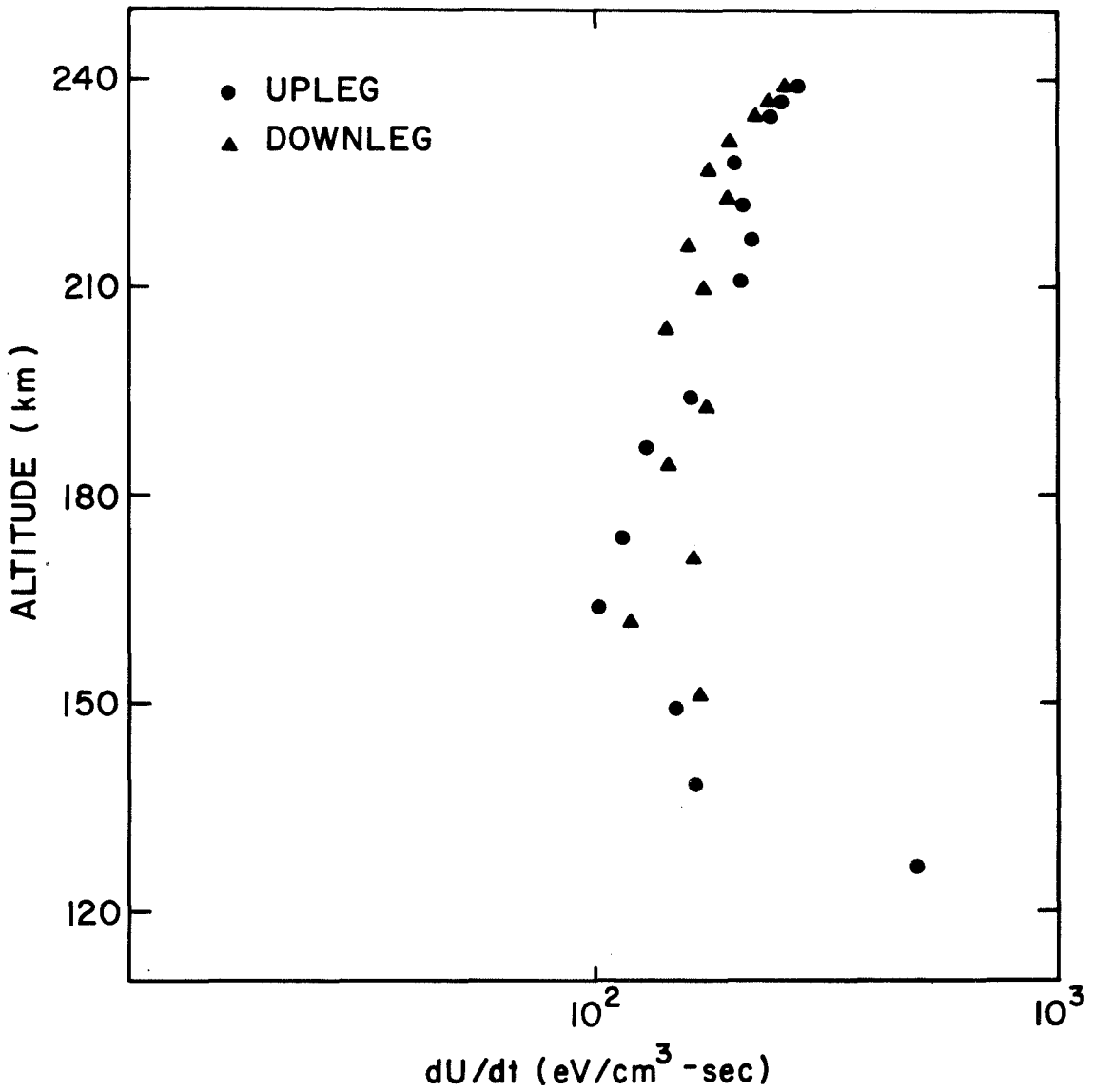

Fig. 3.9 THERMAL ELECTRON COOLING RATE BY ELASTIC COLLISION WITH O.

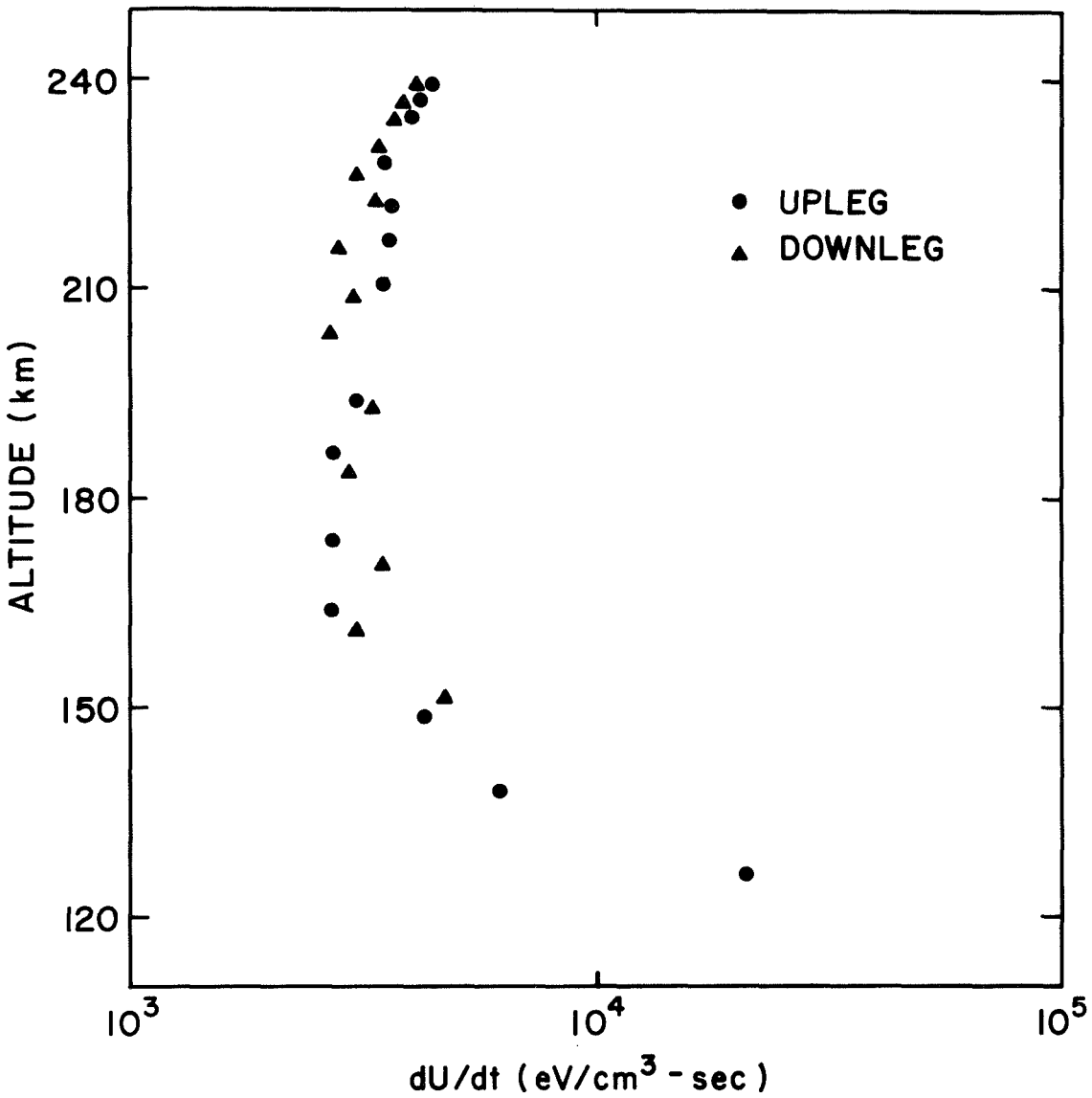

Fig. 3.10 THERMAL ELECTRON COOLING RATE BY EXCITATION OF FINE STRUCTURE LEVELS OF ATOMIC OXYGEN.

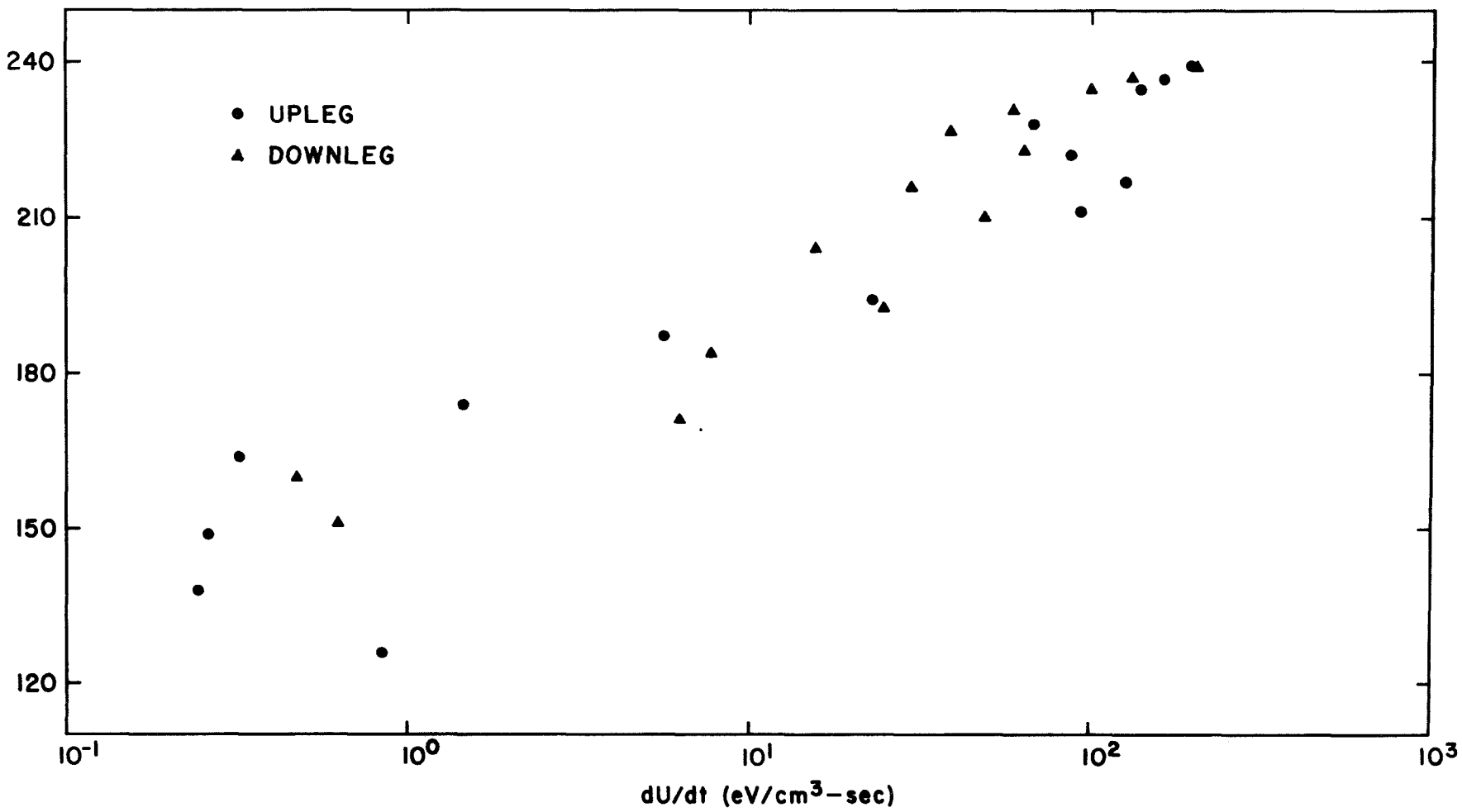

Fig. 3.11 THERMAL ELECTRON COOLING RATE BY EXCITATION OF ATOMIC OXYGEN METASTABLE STATE

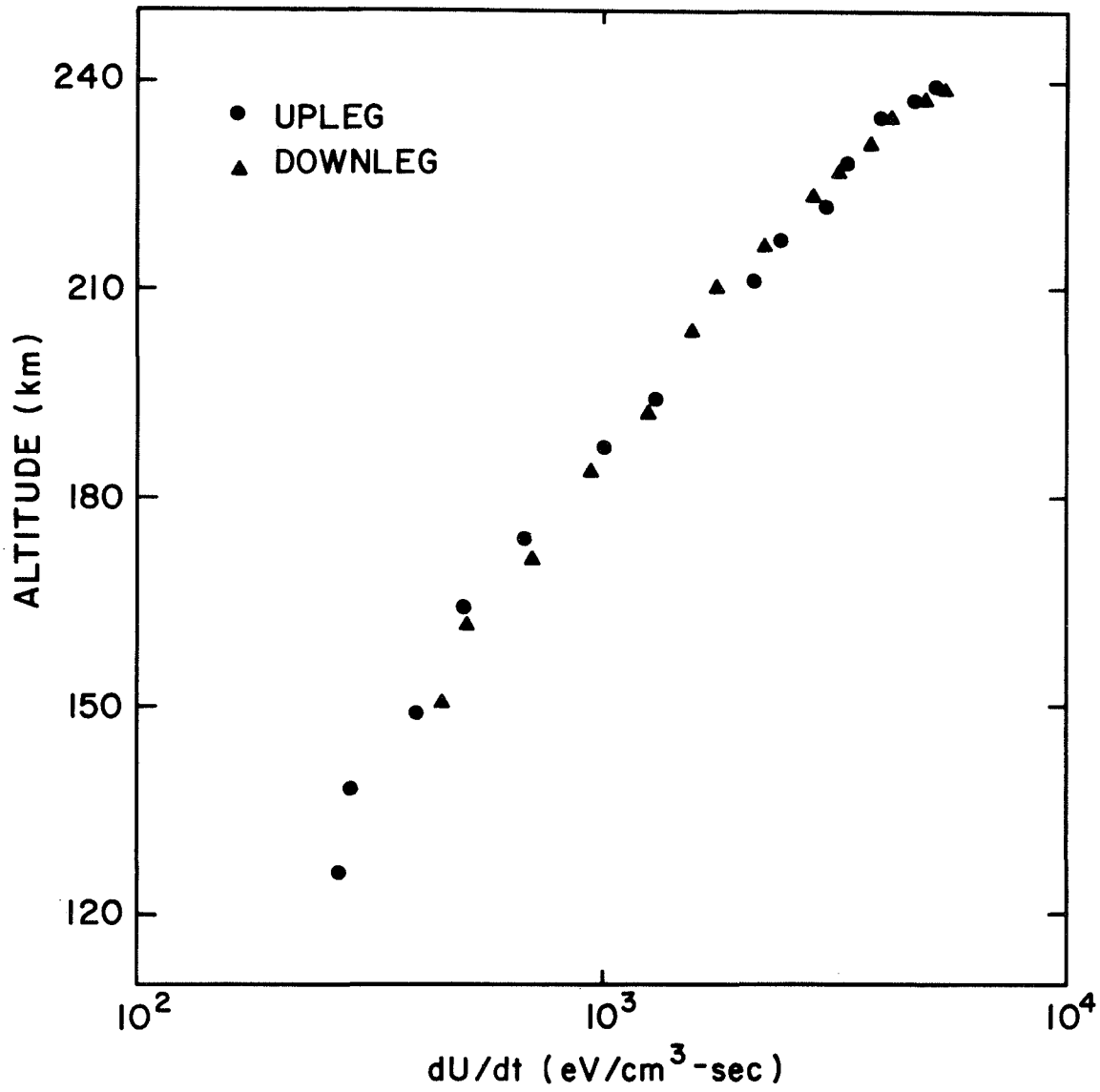

Fig. 3.12 THERMAL ELECTRON COOLING RATE BY ELECTRON - ION COULOMB COLLISION.

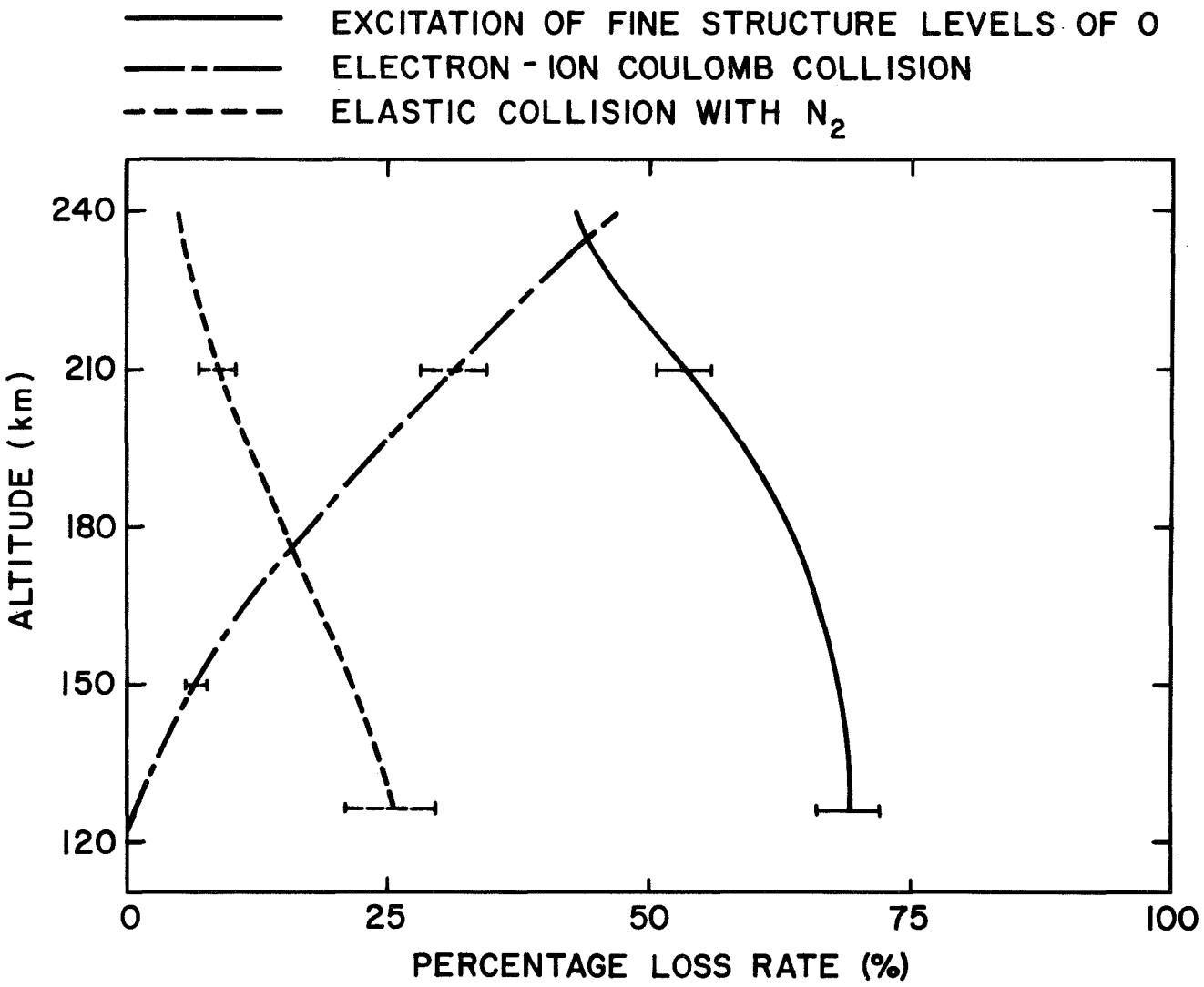

Fig. 3.13 PERCENTAGE LOSSES AND ESTIMATED ERRORS FOR DOMINANT LOSS PROCESSES.

TABLE 3.3: ELECTRON COOLING RATES BY NEUTRAL CONSTITUENTS AND IONS

	Altitude (km)	Electron Cooling Rates (ev/cm^3 - sec) N_2	O_2	O	O_A	O_M	O^+
Ascent	126.	7,990	763.0	494.	22,000	0.83	267.
	138.	1,850	147.0	165.	6,230	0.24	284.
	149.	1,400	99.1	150.	4,490	0.26	390.
	164.	726	44.4	103.	2,700	0.32	502.
	174.	684	38.3	114.	2,660	1.45	679.
	187.	599	32.1	129.	2,740	5.66	983.
	194.	679	35.0	163.	3,140	23.0	1280.
	211.	617	30.7	209.	3,600	93.0	2090.
	217.	579	28.5	218.	3,640	125.0	2410.
	222.	494	23.4	207.	3,530	87.3	3040.
	228.	436	20.2	201.	3,480	67.5	3340.
	235.	473	21.1	239.	3,940	139.0	4040.
	237.	493	21.9	253.	4,140	164.0	4450.
	239.	508	21.4	265.	4,280	199.0	4670.
Descent	151.	1,550	105.0	169.	4,800	0.63	446.
	162.	855	52.5	120.	3,150	0.47	508.
	171.	1,010	60.5	164.	3,640	6.30	703.
	184.	697	37.7	144.	3,020	7.72	935.
	193.	703	36.9	175.	3,370	24.6	1260.
	204.	482	23.9	143.	2,760	15.6	1560.
	210.	521	25.7	172	3,070	47.9	1770.
	216.	434	21.0	160	2,930	29.5	2230.
	223.	466	22.0	194	3,380	63.6	2930.
	227	393	17.8	177	3,170	38.9	3200.
	231.	419	18.8	197	3,440	58.9	3700.
	235.	439	19.4	222	3,760	99.6	4010.
	237.	463	20.2	242	4,010	132.0	4430.
	239.	513	21.7	268	4,310	209.0	4680.

different temperatures. These facts may suggest that the secondary electron distribution in the altitudes below 180 km are closer to a Maxwellian distribution than distributions of the secondary electrons above 180 km.

In calculating electron energy losses to neutral constituents, it is necessary to take into account the uncertainties existing in the neutral density measurements in the atmosphere. Since neutral densities vary at different places around the world and at different times of the year, it is difficult to choose a model neutral densities profile which represents the atmospheric density prevailing at Wallops Island, Virginia, when the experiment was performed. Recently Hedin et al. (1970) have pointed out the fluctuations up to 20 percent of neutral densities can exist in the atmosphere and that fluctuations of atmospheric density may be related to the gravity waves in the upper atmosphere. Gravity waves are very low frequency atmospheric waves. Mathematically, the existance of these waves is derived from gravity terms in the equation of motion. At present, the physical sources of these waves are still not known. They may be: (1) turbulence in the lower atmosphere, or (2) perturbations of the wind caused by mountains. Other possible sources may be thunderstorm activity and nuclear explosions.

In this investigation, the calculated electron energy loss rate was largely affected by the losses due to excitation of the fine structure levels of atomic oxygen. Therefore, the number density of atomic oxygen chosen for calculating the energy loss rate would have affected significantly the accuracy of the calculated energy balance. Due to the fluctuation of neutral density as pointed out by Hedin et al. (1970), density fluctuation could have caused an error of approximately 10 percent in the calculated energy loss rate. The energy losses due to elastic collision of electrons with N_2 and O_2 represented only a small portion of the total energy losses; therefore, the variation of N_2 and O_2 densities in the upper atmosphere could have affected the calculated energy loss rate only slightly.

The energy loss by vibrational excitation of nitrogen molecules has been studied by Dalgarno et al. (1968) following the procedures described by Rees et al. (1967). According to their calculations, this process may be a dominant energy loss mechanism for electrons in the energy interval of roughly 1.7 to 3.5 ev; therefore, the energy distribution function in this region should show a strong perturbation. Hoegy et al. (1965) and Shea et al. (1968) included this vibrational loss process in deriving the energy distribution function for photoelectrons and showed a deep valley in the distribution function around 2 ev region. Since their calculations were based on the momentum transfer cross-section measured in the laboratory, their

opinions on vibrational energy loss in the upper atmosphere are a matter of controversy. In this experiment, the retarded probe current collected showed two distinct linear regions (Figure 2.4) when the current was plotted on a logarithmic scale. If the energy losses due to vibrational excitation of molecular nitrogen were taken into account in this investigation, the total energy loss rate would increase by 100 percent as shown in Figure 3.14, and its effect upon the distribution function could be shown on the current collected by the probe. The data obtained by this experiment, however, did not show such perturbation in the energy distribution function between 1.7 and 3.5 ev as calculated by Hoegy et al. (1965) and Shea et al. (1968). As a result, it may be suggested that the vibrational energy loss process does not have a large effect on the electron energy distribution function in the altitude ranges between 120 and 240 km. For this reason, the vibrational energy loss by molecular nitrogen has not been adopted in this dissertation.

Estimated errors for energy losses vary according to the processes involved. The most important energy loss mechanism between 120 and 230 km is the excitation of fine structure levels of atomic oxygen, and the accuracy of the loss rate depends upon the cross-section adopted. Herman and Chandra (1970) have estimated that their calculated loss rate may vary approximately 5 percent. As a result,

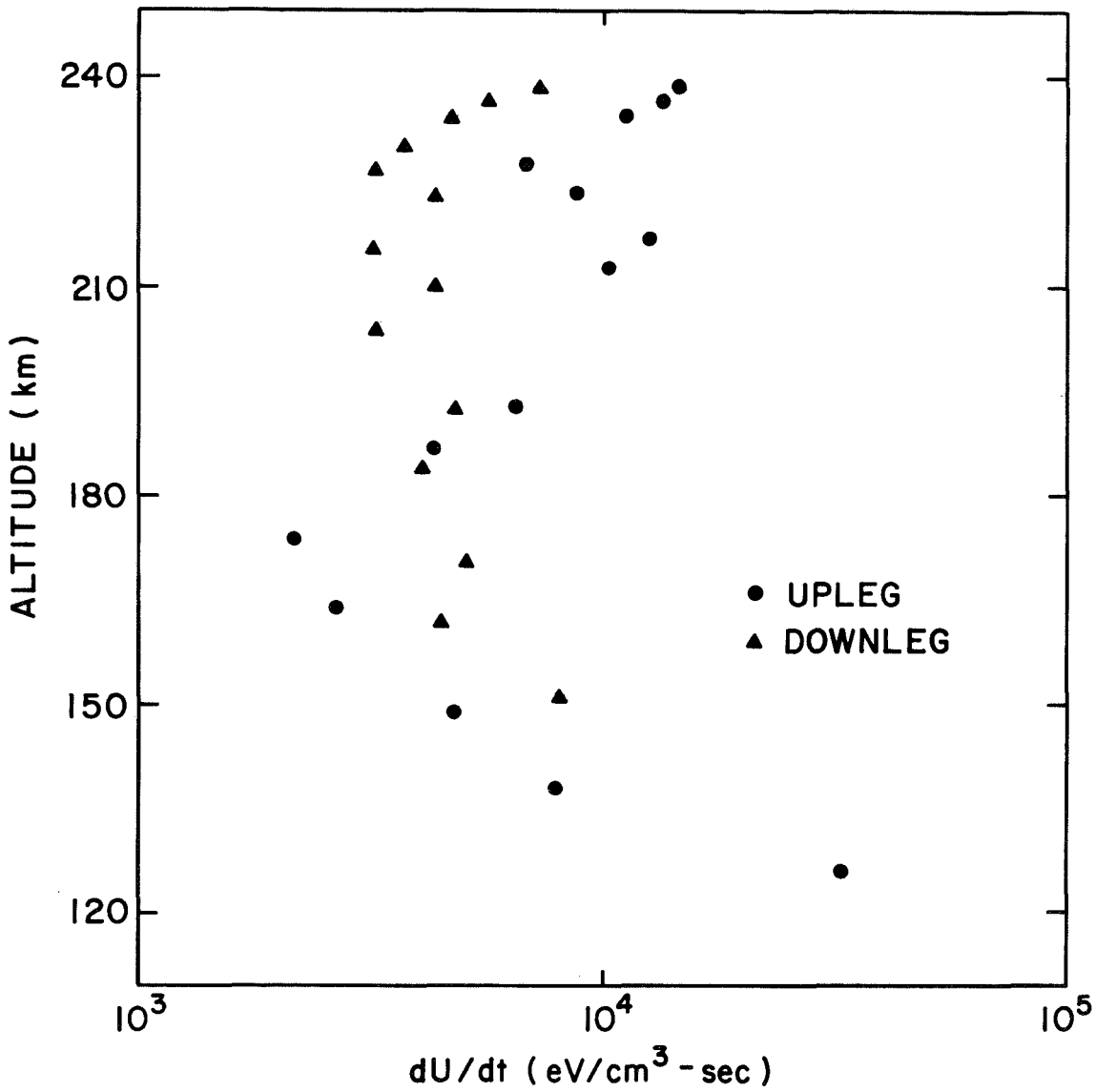

Fig. 3.14 THERMAL ELECTRON COOLING RATE BY EXCITATION OF VIBRATIONAL STATE OF N_2

an error of approximately 3 percent could occur in the calculated loss rates. Elastic collision of electron with molecular nitrogen at lower altitudes (~130 km) can cause an energy loss rate of approximately 30 percent. The uncertainty of the cross-section in this process is believed to be within 15 percent. An error of approximately 5 percent could apply in this case. Electron-ion coulomb collision at higher altitudes (~235 km) dominate 50 percent of the total loss rate, the accuracy of the electron-ion coulomb collision cross-section is estimated to be approximately 10 percent (Banks, 1966). Therefore, the optimum estimate of error for the calculated total heat loss rate is 10 - 20 percent. Estimations of errors for the individual processes have been calculated for the different altitudes, and the results are plotted in Figure 3.13.

CHAPTER IV

The Production of Superthermal Electrons

A. Introduction

The primary objective of this investigation is to study the energy distributions of electrons in the energy range from 0 to 15 ev in the middle ionosphere. To accomplish this objective, the author developed a theoretical model of the electron energy distributions in the above energy range. In developing his model, the author did not accept the premise that the vibrational excitation of molecular nitrogen in the ionosphere represents an important mechanism of energy losses for electrons. In this study, superthermal electrons refer to those electrons with energies greater than ~ 1 ev, without particular reference to their source of origin. It is believed that the main sources of these superthermal electrons are primary photoelectrons and secondary electrons produced by the primary photoelectrons. At least some superthermal electrons are produced through superelastic collisions in which the energy of electrons is increased by interactions with either ions or neutrals in excited or metastable states.

If it is assumed that photoelectrons are the dominant portion of superthermal electrons, then it can be expected that at high energies the superthermal electron energy

distributions would approximate the primary photoelectron distribution. Calculations for the energy distribution of photoelectrons have been done by Hoegy, et al. (1965), Shea, et al. (1968), and Dalgarno, et al. (1969). They all use the solar flux data provided by Hinteregger, et al. (1965) as the source for the production of photoelectrons, but have adopted different cross-sections and weighting factors for loss processes. The process of the production of secondary electrons has remained a problem. Green and Barth (1967) mentioned it in their calculations, but the problem has not been completely investigated.

The equilibrium energy distribution function is expressed as:

$$F(E) = -\frac{P(E)}{\frac{dE}{dt}} = -\frac{\int_E^\infty p(E')dE'}{\frac{dE}{dt}} \tag{4.1}$$

where $\frac{dE}{dt}$ is the energy loss rate of the photoelectrons, and P(E) is the accumulated production rate defined by

$$P(E) = \int_E^\infty p(E')dE' \tag{4.2}$$

and where $p(E')\,dE'$ is the rate at which photoelectrons are produced in the energy interval E' and $E' + dE'$. In this chapter the equilibrium energy distribution will be calculated by using the above equation. Discussions will be made concerning the accumulated production rate $P(E)$ and the energy loss rate $\frac{dE}{dt}$. Also included will be a possible explaination of the linear section of the probe current described in Figure 2.4. In addition, some of the calculated results and discussions will be presented.

B. Production of Photoelectrons

Energetic electrons are produced in the upper atmosphere by absorption of extreme ultraviolet solar radiation (EUV). In thermospheric physics, the EUV refers mainly to the range of wavelengths from about 1750 Å to 170 Å, together with X-rays, including both soft and hard, but generally not referring to γ-rays. Photons with energies greater than about 12 ev can ionize one or more of the major atmospheric constituents are tabulated in Table 4.1. The energy of ejected photoelectrons depends on the energy of the incident photon and the ionization potential of the target atom. Tohmatsu, et al. estimated that about two-thirds of EUV energies are used in removing electrons from atmospheric molecules. The remaining one-third are transferred to the kinetic energy of the ejected photoelectrons.

TABLE 4.1

Ionization Potentials for Photoionization of Atoms and Molecules

	First Ionization Potential (ev)
NO	9.25
O_2	12.08
H	13.59
O	13.61
N	14.54
N_2	15.58
He	24.56

In order to calculate the accumulated production rate P(E) for the primary photoelectrons, it is necessary to know the probability of ionization in each of the electronic states of ions in addition to the ionization cross-sections. Tohmatsu, et al. (1965) performed a calculation of the kinetic energy spectrum of the primary photoelectrons. The solar flux data, ionization cross-sections, and absorption cross-sections were compiled by Hinteregger, et al. (1965). Tohmatsu, et al. (1965) also calculated the photoelectron production rates for different solar zenith angles and for several different altitudes ranging from 150 km to 500 km. For calculations in this study, the solar zenith angle $\sim 30^{\circ}$ was used, and the accumulated photoelectron production rate can be written as:

$$P(E) = P_o \exp(-E/E_o) \tag{4.3}$$

where P_o represents the total production rate, and E_o is the mean kinetic energy of the photoelectrons. The mean energy of the primary photoelectrons is approximately constant at ~ 10 ev above 200 km. Below 200 km, the mean energy becomes large due to the increasing importance of He II 304 Å emission. The mean kinetic energy for the photoelectrons used in this calculation was taken from Tohmatsu, et al. (1965) and tabulated in Table 4.2.

TABLE 4.2

Total Production Rates and Average Kinetic Energy for Photoelectrons

Altitude (km)	Total Production Rate (cm^{-3})	Average Kinetic Energy (ev)
150	6,000	15
200	2,000	10
240	700	10

Photoelectron production depends upon the EUV solar photons in the upper atmosphere. The total production rates as a function of altitude have been derived by Hinteregger, et al. (1965) and are reproduced in Figure 4.1. The figures for the total production rate and mean kinetic energy for the photoelectrons used in the calculations in this study are shown in Table 4.2. By utilizing equation (4.3), the accumulated production rate for the photoelectrons as a function of energy can be derived. The production rates for several different altitudes are plotted in Figure 4.2.

C. Cooling Processes of Photoelectrons

Photoelectrons lose energy by exciting and ionizing the neutral particle constituents of the atmosphere and by elastic collisions with the ambient thermal electrons. Elastic collisions with neutral particles absorb a negligible portion of the photoelectron energy.

Energy loss due to collision with ambient electrons can be readily estimated by equation (3.1). When the energies of the photoelectrons are substantially greater than those of thermal electrons, equation (3.1) can be simplified and written as:

$$\frac{dE}{dt} = 1.16 \times 10^{-4}\ n_e\ E^{-\frac{1}{2}} \quad \text{ev/sec} \qquad (4.4)$$

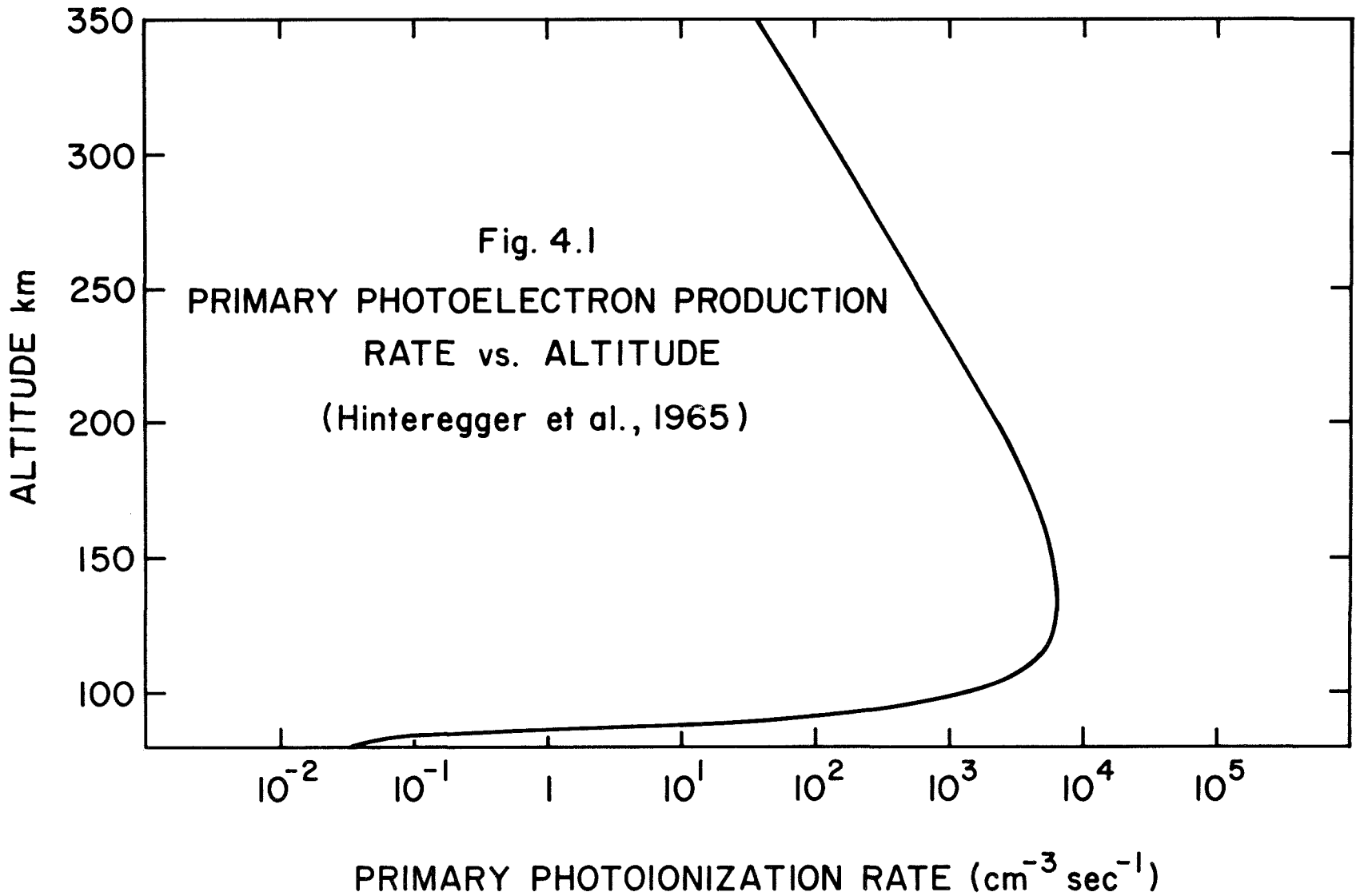

Fig. 4.1
PRIMARY PHOTOELECTRON PRODUCTION RATE vs. ALTITUDE
(Hinteregger et al., 1965)

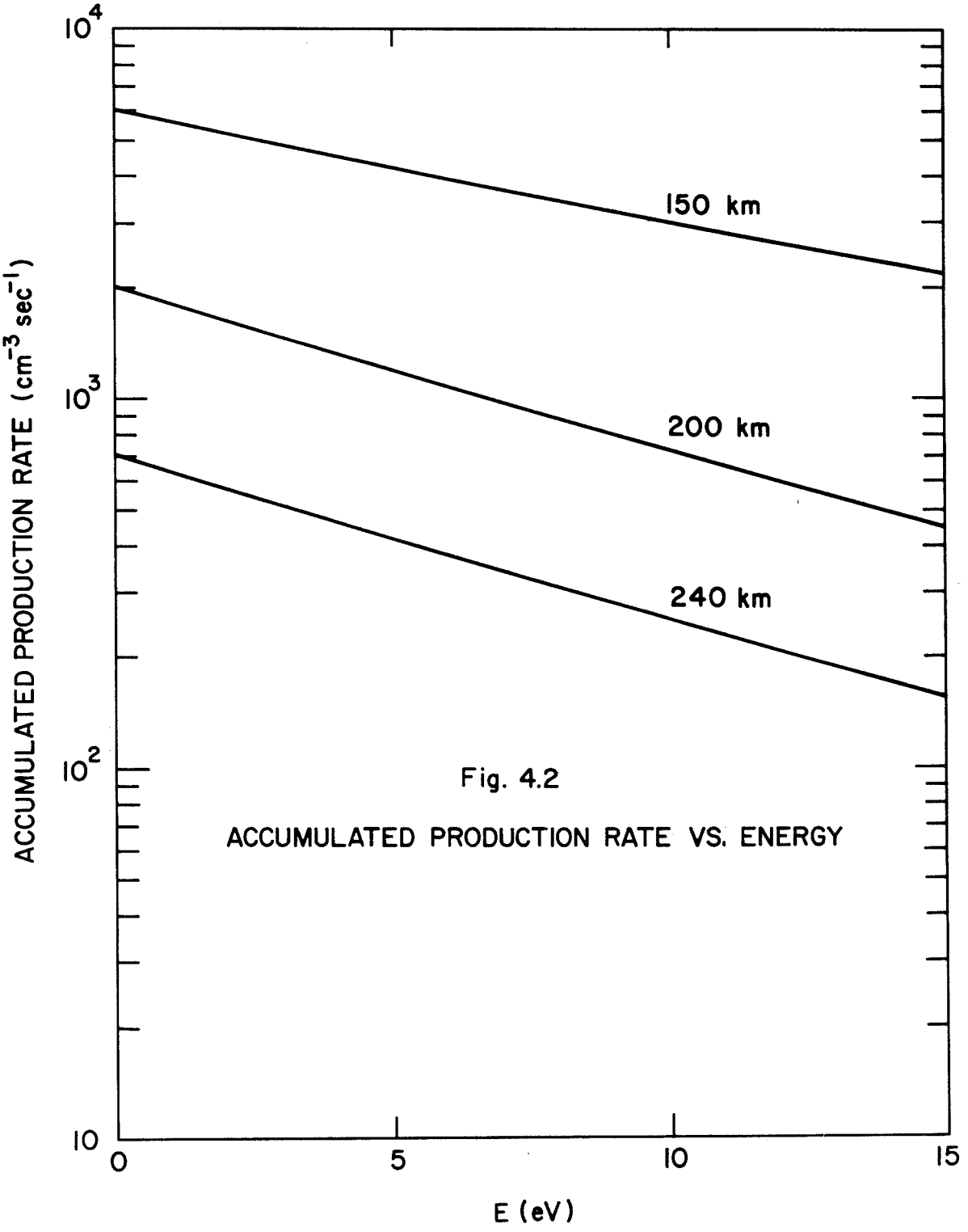

Fig. 4.2

ACCUMULATED PRODUCTION RATE VS. ENERGY

where E is the fast electron energy in ev.

The rate of energy loss of photoelectrons due to inelastic collisions with a neutral species n(m) is shown in the equation:

$$\frac{dE}{dt} = n(m)\ E\ Q_D\ v \quad \text{ev/sec} \tag{4.5}$$

where n(m) is the number density of the neutral species, E and v are the energy and the magnitude of the velocity of the photoelectron, and Q_D is the momentum transfer cross-section.

In measurements used in this study, the secondary energy distribution were devoid of the structure suggested by Hoegy, et al. (1965), and Shea, et al. (1968). The two groups suggested a depression in the distribution curves at about 3 ev is related to the vibrational excitations of N_2, and a simultaneous decrease in vibrational and electronic excitation energy losses should be the cause of the hump between 5 and 6 ev. Due to the uncertainties in determining the inelastic collision cross-sections for N_2, O_2, and O, it is extremely difficult to adopt a set of reliable cross-sections. Calculations used in this study depict a smooth photoelectron energy distribution curve devoid of structure based on the energy loss rate of electrons to the neutrals as presented by Shea, et al. (1968).

The calculated energy loss rates of superthermal electrons due to inelastic collisions with neutral particles and elastic collisions with thermal electrons are shown in Figures 4.3 and 4.4. The total time rates of energy loss are given in Figure 4.5. From these curves it can be seen that at an altitude of 150 km the energy loss to the neutrals is more important than the electron-electron loss. At 240 km the electron-electron energy loss becomes the dominant loss for electron energy below 5 ev. Above 5 ev, the inelastic losses always are the important loss for photoelectrons.

D. Equilibrium Energy Distributions of Superthermal Electrons

Apart from the thermal electron gas, electrons with energies greater than approximately 1 ev are called "superthermal electrons." In this study it was assumed that they were originally all primary photoelectrons. Based on this assumption, a formal expression for the equilibrium energy distribution function can be constructed as follow:

$$p(E)dE = F(E)\frac{dE}{dt} \,/\, E - F(E)\frac{dE}{dt} \,/\, E+dE = - d\left[F(E)\frac{dE}{dt}\right] \qquad (4.6)$$

or

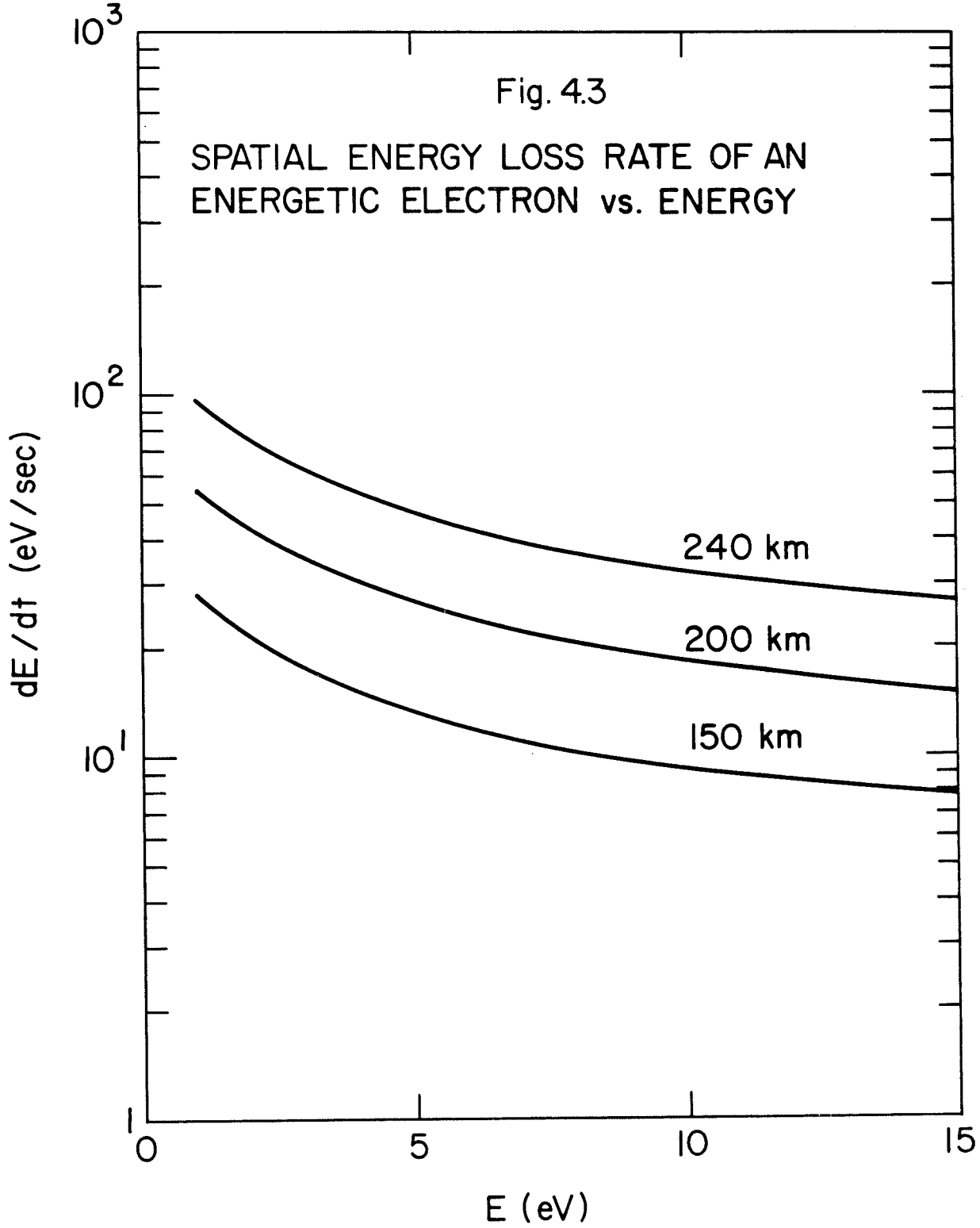
Fig. 4.3
SPATIAL ENERGY LOSS RATE OF AN ENERGETIC ELECTRON vs. ENERGY
10^3
10^2
10^1
1
dE/dt (eV/sec)
240 km
200 km
150 km
0
5
10
15
E (eV)

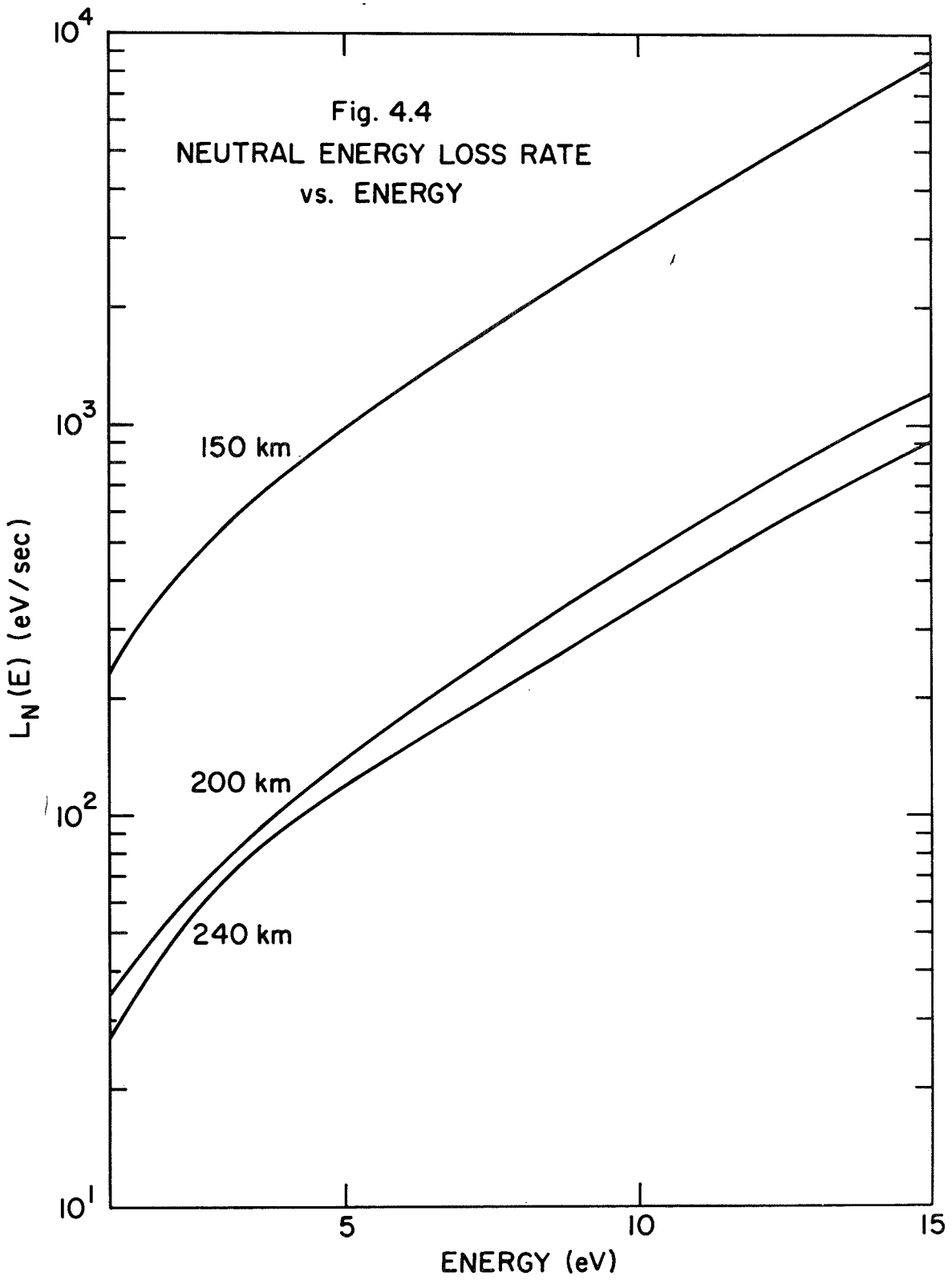
Fig. 4.4
NEUTRAL ENERGY LOSS RATE
vs. ENERGY
150 km
200 km
240 km
10^4
10^3
10^2
10^1
$L_N(E)$ (eV/sec)
5
10
15
ENERGY (eV)

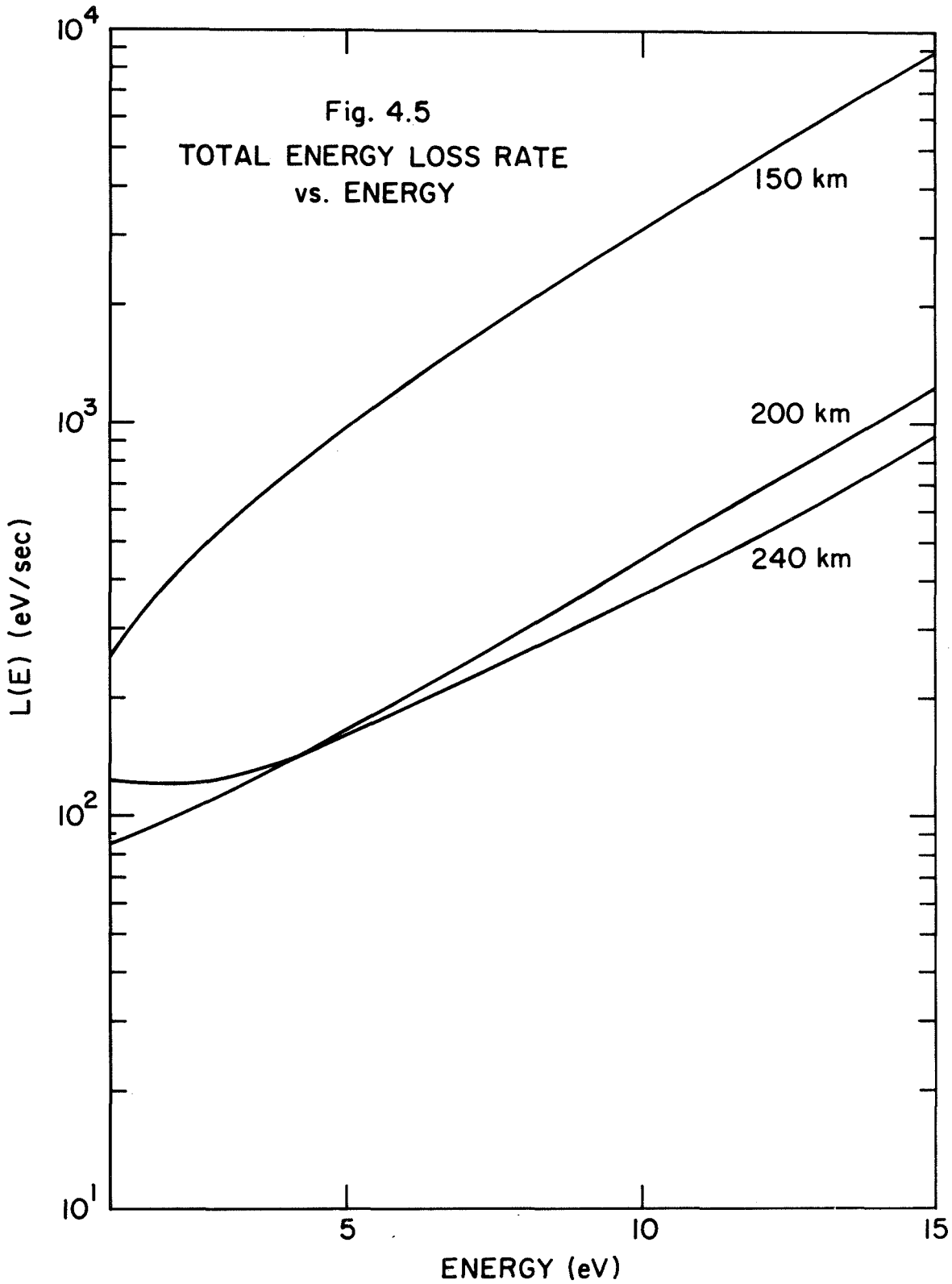
Fig. 4.5
TOTAL ENERGY LOSS RATE
vs. ENERGY
150 km
200 km
240 km
10^4
10^3
10^2
10^1
L(E) (eV/sec)
5
10
15
ENERGY (eV)

$$F(E) = - \frac{\int_{E}^{\infty} p(E')dE'}{\frac{dE}{dt}} \tag{4.7}$$

Both the accumulated production rate and the energy loss rate have been calculated in Sections B and C of this chapter. Hence, by using equation (4.7) the distribution function F(E) can be obtained immediately. It has been calculated for several different altitudes, and the results are shown in Figure 4.6.

Comparisons of the electron energy distribution function published by Shea, et al. for 156 km (1968), Hoegy, et al. and Nagy and Fournier for 160 km (both 1965), and the calculated results for 150 km are plotted in Figure 4.7. The main difference between the calculated results achieved in this study and the results published by the two groups above are indicated by the existence of the trough around 3 ev and the hump around 5 ev, due to vibrational loss processes, of the energy distribution function.

In Section A of Chapter II, it was shown that the energy distribution function F(E) can also be evaluate by taking the second derivative of the probe current

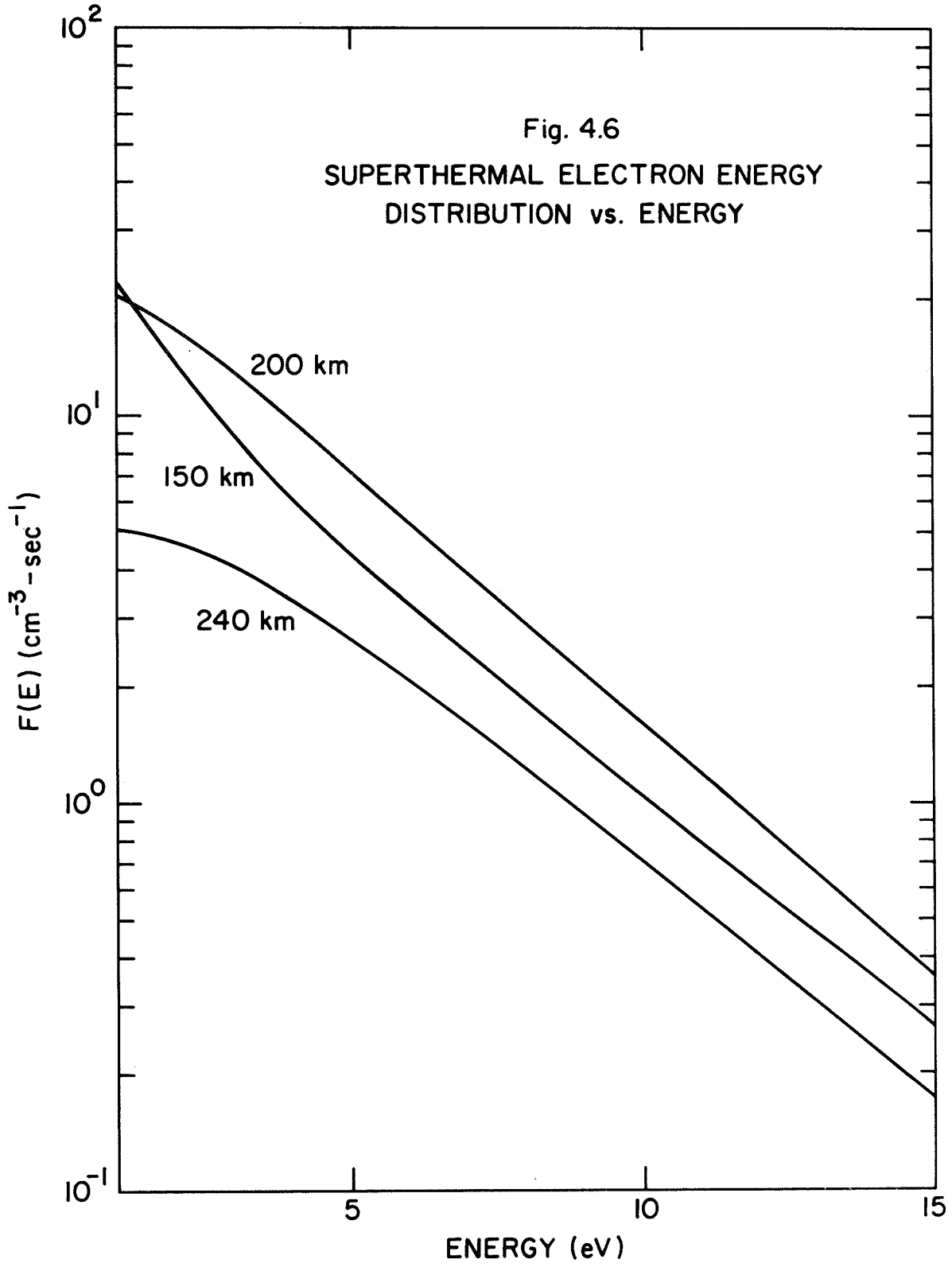
Fig. 4.6
SUPERTHERMAL ELECTRON ENERGY
DISTRIBUTION vs. ENERGY
200 km
150 km
240 km
10^2
10^1
10^0
10^{-1}
F(E) (cm^{-3}-sec^{-1})
5
10
15
ENERGY (eV)

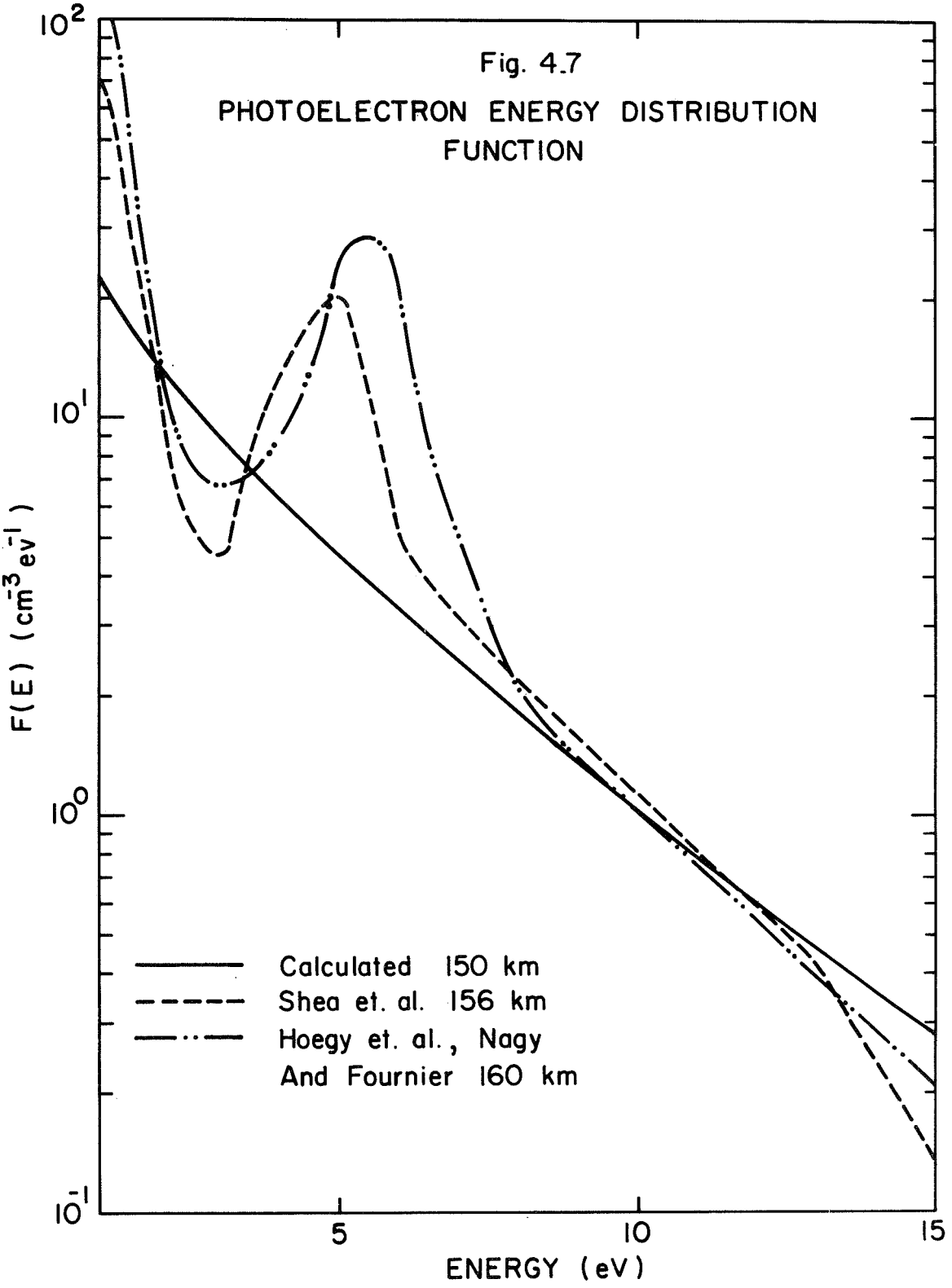
Fig. 4.7
PHOTOELECTRON ENERGY DISTRIBUTION FUNCTION
10^2
10^1
10^0
10^{-1}
F(E) ($cm^{-3} ev^{-1}$)
5
10
15
ENERGY (eV)
Calculated 150 km
Shea et. al. 156 km
Hoegy et. al., Nagy And Fournier 160 km

(Druyvesteyn relationship). It is difficult to maintain accuracy in performing the graphical differentiation without smoothing the raw data. Therefore no attempt was made to obtain the distribution function F(E) by using this method.

E. Delta Function in the Distributions

In a typical section of the i-V curve, as shown in Figure 2.5, the current appears to be relatively linear with applied retarding potential in the range of 6 - 13.5 volts. Since the second derivative of the current with respect to the applied voltage is nearly zero in this region, according to the Druyvesteyn relationship given in Section A of Chapter II, it may be concluded that relatively few electrons exist in the energy interval between 8 and 15 ev. The recorded current in this range of retarding potential could be due mainly to electrons with energies greater than 15 ev. In order to produce a linear current in the energy interval between 8 and 15 ev, a particular distribution function, which is different from the exponential form is needed. It can be assumed that electrons with energies greater than ~ 15 ev are approximately monoenergetic with energy E_o. Based on this assumption, the current due to the delta function can be derived.

By using the notations defined in Section B of Chapter II, the current related to the delta function may be written as:

$$i' = 2\pi a l e \int_{-V_{max}}^{V_{max}} dv \int_{\alpha}^{\sqrt{c^2 - V^2}} v_\rho f(v_\rho, v)\, dv_\rho \tag{4.8}$$

where $V_{max} = \sqrt{\left(\frac{R}{a}\right)^2 (v_o^2 - \frac{2eV}{m})}$, v_o is the magnitude of velocity of the monoenergetic particles with energy E_o, and the distribution function can be expressed as:

$$f(v_\rho, v) = \begin{cases} n_o/(2\pi v_o^2 \sqrt{1 - \frac{v_\rho^2 + v^2}{v_o^2}}) , & v_\rho^2 + v^2 \leq v_o^2 \\ 0 & v_\rho^2 + v^2 > v_o^2 \end{cases} \tag{4.9}$$

and satisfied the normalization condition

$$\int_o^{V_o} dv \int_{-\sqrt{C^2 - V_\rho^2}}^{\sqrt{C^2 - V_\rho^2}} dv_\rho \; f(v_\rho, v) = n_o \tag{4.10}$$

and where n_o is the particle density for electron with energy E_o.

The current i' due to the delta distribution can be derived by substituting equation (4.9) into equation (4.8).

$$i' = 2\pi a l n_o e \int_{-V_{max}}^{V_{max}} dv \int_{\alpha}^{\sqrt{c^2 - V^2}} v_\rho/(2\pi v_o^2 \sqrt{1 - \frac{v_\rho^2 + v^2}{v_o^2}})\, dv_\rho \tag{4.11}$$

$$= \frac{\pi R l n_o e v_o}{2} (1 - \frac{eV}{E_o}) \tag{4.12}$$

The current i' due to the delta function in the equilibrium distribution is a function of the probe radius and the applied potential, and also depends on the value of E_o. For a given E_o, it is possible to calculate the current as a function of the applied retarding potential for a given probe with radius R. The relation of the current and the retarding probe potential has been calculated for probe radius equals to 1 cm, with E_o equals to 25 ev, and the results are shown in Figure 4.8.

F. Results and Discussion

From Figure 4.6 it can be seen that above 3 ev the distribution function F(E) is an exponentially decreasing function of energy. By integrating the area below the distribution curves, it should be possible to calculate approximately the superthermal electron density. At 150 km and 200 km, the integrated values are approximately 100 electrons/cm^3. These values are comparable to the measured superthermal electron concentrations. At 240 km, the calculated value is approximately $\sim$50 electrons/cm^3, while the measured density is 4 to 5 times larger. This fact may suggest that photoionization by incident solar radiation is not the only source for these energetic electrons.

The concentration of electrons with energies greater than 15 ev increases from $\sim$5 electrons/cm^3 at altitudes of approximately 150 km to $\sim$15 electrons/cm^3 at about

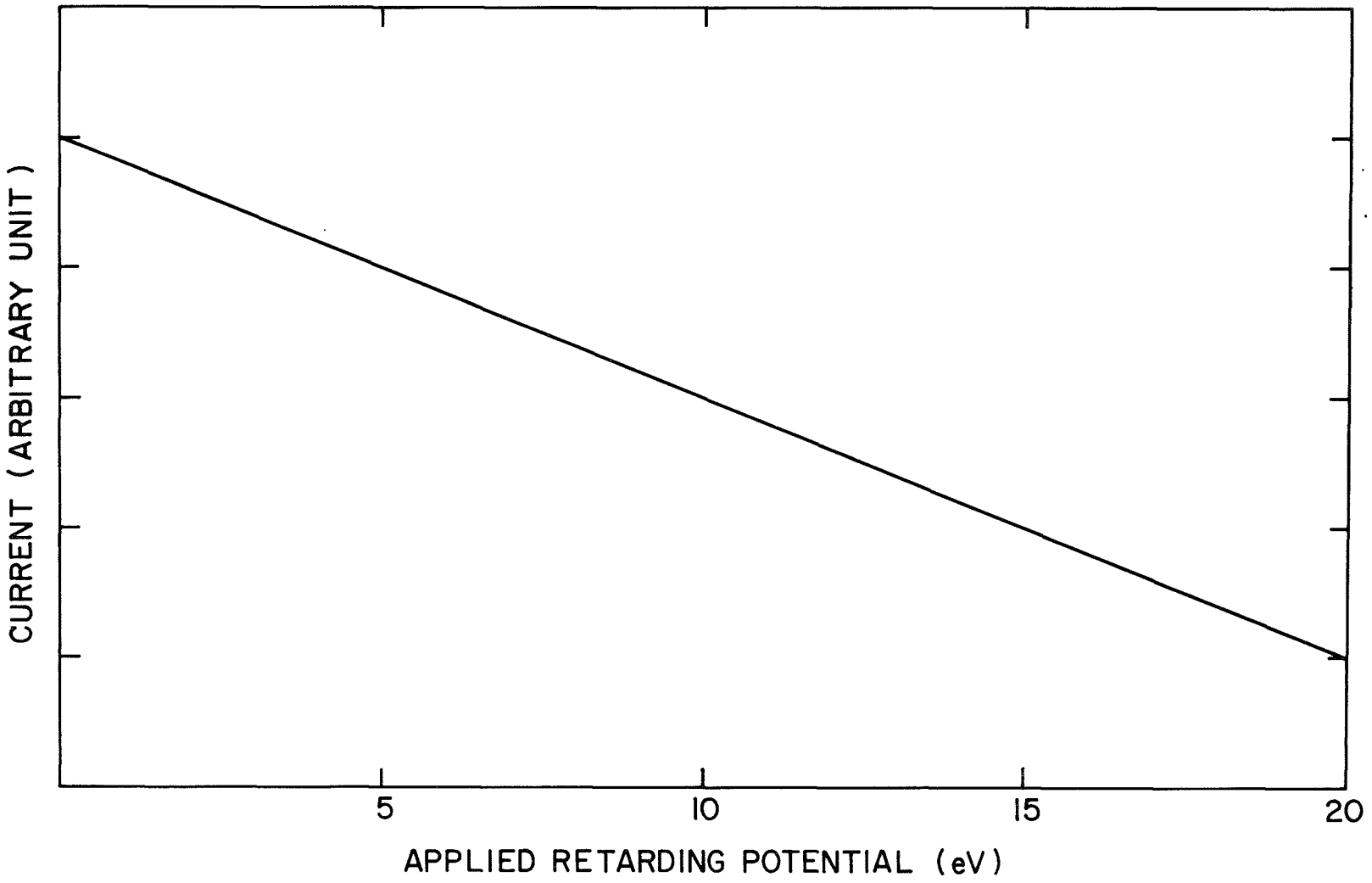

Fig. 4.8 CURRENT DUE TO DELTA FUNCTION ON EQUILIBRIUM ENERGY DISTRIBUTION

240 km. Figure 4.6 shows that the energy distribution function for 150 km is larger than that for 240 km. An extrapolation would indicate that the concentration of electrons with energies greater than 15 ev would not be larger at 240 km than at 150 km. This difficulty can be resolved by superimposing the delta function on the energy distribution. By choosing different electron densities for electrons with 25 ev energy at 150 km and at 240 km, this problem can be avoided.

The uncertainty in the measurements of the EUV solar spectrum will also affect the calculations significantly. The solar spectrum measurements used in this study which were taken by Hinteregger, et al. in (1965), were subjected to variations in place and time. Several Orbital Solar Observatory satellites put into orbit since 1962 should eventually provide better data on the solar EUV spectrum measurements, although, up to the present time no data have been released.

It has been shown that when the ejected primary photoelectron has a kinetic energy greater than the ionization potentials of the atoms or molecules it encounters, the production of secondary electrons occurs. When electrons have energies greater than 70 ev, they produce one ion-pair for every $\sim$ 34 ev. Electrons with energies between 70 ev and 20 ev may produce one ion-pair. Dalgarno, et al. (1963)

indicated that at approximately 120 km the majority of the photoelectrons being produced have energies between 60 and 120 ev. Above 150 km, the production spectrum is dominated by photoelectrons produced in the energy interval of 25 to 35 ev. Therefore, it can be assumed that the secondary electrons produced by primary photoelectrons may contribute substantially to the total electron production. Theoretical considerations concerning the energy distributions of the secondary electrons must begin with a careful examination of the relevant cross-sections of the production processes. This examination should include the study of impact ionizations, superelastic collisions, and inelastic collisions. Experimental data are available concerning impact ionization and inelastic collisions by electrons for N_2, O_2, and O, but these measured cross-sections usually are not very accurate. Under these conditions, the secondary electron distribution requires further investigation.

Figure 4.7 shows that a monoenergetic distribution will produce a linear section of current on the i-V plot. In the altitude ranges used in this investigation, the particle-particle interactions do not seem to be the cause of the delta function in the energy distributions. One possible reason for the existence of a monoenergetic distribution is the interaction of wave-particle in the ionosphere (Sinha, 1970). The emerging energetic electrons interact with electromagnetic waves in the ionosphere to form a steady peak in the energy distribution.

CHAPTER V

Summary and Conclusions

A. Summary

1. Results of Calculations

The energy balance of electrons in the middle ionosphere can be calculated by using measured superthermal and thermal electron densities and temperatures, in combination with the model atmosphere and electron collision cross-sections. In the calculations used in this study, the heat input rates for superthermal electrons to thermal electrons are found to be in the range between 3×10^3 ev/cm^3-sec and 1.5×10^4 ev/cm^3-sec. The numbers in this range correlate closely with the calculated total heat loss rate for electrons to ions and neutral constituents. The deviation for heat loss and input becomes noticeable to approximately 235 km, which is close to the apogee (239 km) for the rocket flight which provided data used in this investigation.

In the rocket flight, the measured superthermal electron densities were approximately 150 - 200 electrons/cm^3 of heights between 150 and 200 km. In this altitude range, the number density of superthermal electrons corresponded to ~ 0.02 percent of the thermal electron density. This may suggest that superthermal electrons at varying heights in this altitude range were produced by similar physical

processes. By assuming a photoionization origin for superthermal electrons, it was possible to calculate the equilibrium energy distribution function.

For electrons with thermal energy, electron-ion collisions and elastic collisions with neutral constituents are the dominant energy loss processes. Below 300 km, the elastic collisions constitute the dominant energy loss processes for thermal electrons. Inelastic collisions and ionization are the most important energy loss processes for the superthermal electrons throughout the altitude range of this study.

2. Possible Errors in the Calculations

The overall correlation between the heat input rate for superthermal electrons to thermal electrons and the heat loss rate for thermal electrons to neutral constituents and ions is gratifying. A large number of theoretical studies and experimental works have been carried out to improve the accuracy of collision cross-sections. Most of the collision cross-sections concerning processes in the ionosphere are measured under laboratory conditions which are far different from those found in the ionosphere. For example, the measurements of the momentum transfer cross-section for molecular nitrogen were performed in a container filled with pure nitrogen gases, while in the ionosphere besides nitrogen molecules there exist oxygen atoms and

oxygen molecules. Recently, Breshears and Bird (1968) reported in an experiment which measured the vibrational relaxation time for molecular nitrogen that the existence of atomic oxygens would decrease the relaxation time by nearly two order of magnitude, in a comparison of values measured in pure nitrogen. This phenomenon shows that the physical parameters in the ionosphere may be considerably different from those measured in laboratory experiments. For a better understanding of the energy balance in the ionosphere, it is desirable to measure collision cross-sections under ionospheric conditions.

Another source of possible experimental error may arise if a component of the measured flux consisted of photoelectrons originating on surfaces of rockets. It is extremely difficult to evaluate these photoelectrons quantitatively. In Huang's experiment, the pulse probe was mounted $\sim$ 20 in. above the main payload section. Hence, the rocket electrons would require a large angle scatter to be collected by the pulse probe. The probability that electrons undergo a large angle scattering should be small, and can be neglected in this calculation. The average energy for electrons from an aluminum surface exposed to sunlight in the upper atmosphere is approximately 0.2 ev, with electrons seeming not to affect the concentration of measured superthermal electrons. In the experiment, the

photoelectrons from the collector were suppressed by a large positive potential bias on the collector and the innermost grid; therefore, they should not have produced an appreciable photoelectron current.

Photoelectrons with several ev energies can travel a large distance before they finally become thermalized. Recently, Heikkila and Winningham (1970) reported that a flux of 10^8 electrons/cm^2-sec for escaping electrons was measured in the midlatitude daytime ionosphere. Their measurements confirmed the fact that the fast electrons could travel a large distance and did not deposit their energy locally. Therefore, this nonlocal heating effect may have had some influence on the results of this study. No quantitative calculations concerning the importance of this effect in the altitude range between 120 and 240 km have been performed. Further study of this problem is highly recommended.

B. Conclusions

The successful pulse probe experiment used in this study detected both the thermal and the secondary electron distributions. These measured values provided an opportunity to calculate the equilibrium distribution of electrons for energies up to 15 ev. To determine the electron energy distribution beyond 15 ev, the applied retarding potential for the probe should be increased to

about 50 ev. Under this circumstance, the calculation of the equilibrium distribution of electrons up to approximately 50 ev can be performed, giving a better understanding of the secondary electron distributions.

The calculated results from measurements taken during the successful pulse probe experiment indicate the following:

1) The total heat input rate of superthermal to thermal electrons fluctuates between 3×10^3 ev/cm^3-sec and 1.5×10^4 ev/cm^3-sec in varying altitudes between 120 and 240 km. These values correspond to the calculated thermal electron heat loss rate.

2) The electron-ion Coulomb collisions dominate the energy loss for thermal electrons above 200 km. The excitation of fine structure levels of atomic oxygen is also an important energy loss process in the altitude range of this study.

3) The equilibrium distributions for electrons constitute an exponential function for electron energies up to 15 ev.

4) The linear probe current corresponding to the retarding potential in the interval 8 to 15 volts can be reproduced by a monoenergetic energy distribution at ~ 25 ev.

A satisfactory description of equilibrium distributions for electrons with energies below 15 ev has been derived through a combination of information concerning atmospheric compositions, solar flux, and cross-sectional data. The theoretical model used in this study assumed that production and energy losses of photoelectrons occurred locally. More sophisticated calculations concerning production and energy losses of photoelectrons in the middle ionosphere could be made possible through the development of a theoretical model which would describe nonlocal electron heating processes. Hopefully this type of model would provide desirable data concerning electron energy balances at altitudes below 250 km.

REFERENCES CITED

L. A. Antonova and G. S. Ivanov-Kholodnyy, "Corpuscular Hypothesis for the Ionization of the Night Ionosphere," Geomagnetism and Aeronomy, 1, 149 (1961)

P. M. Banks, "Collision Frequencies and Energy Transfer - Electrons," Planet. Space Sci., 14, 1085 (1966)

D. R. Bates, "The Temperature of the Upper Atmosphere," Proc. Phys. Soc. (London) B64, 805 (1951)

R. T. Bettinger, "An In Situ Probe System for the Measurement of Ionospheric Parameters," Ph.D. Thesis, University of Maryland, Department of Physics and Astronomy Tech. Rep. No. 277 (1964)

R. T. Bettinger and E. H. Walker, "A Relationship for Plasma Sheaths about Langmuir Probes," Phys. Fluids, 8, 748 (1965)

E. L. Breig and C. C. Lin, "Excitation of the Spin Multiplets of the Ground State of Oxygen by Slow Electron," Phys. Rev., 151, 67 (1966)

W. D. Breshears and P. F. Bird, "Effect of Oxygen Atoms on the Vibrational Relaxation of Nitrogen," The Journal of Chemical Physics, 48, 4768 (1968)

S. T. Butler and M. J. Buckingham, "Energy Loss of a Fast Ion in a Plasma," Phys. Rev., 126, 1 (1962)

REFERENCES CITED
(Continued)

J. W. Cooper and J. B. Martin, "Electron Photodetachment from Ions and Elastic Collision Cross Section for O, C, Cl, F," Physics Review, 126, 1482 (1962)

A. Dalgarno, M. B. McElroy, M. H. Rees, and J. C. G. Walker, "The Effect of Oxygen Cooling on Ionospheric Electron Temperatures" Planet. Space Sci. 16, 1371 (1968)

A. Dalgarno, M. B. McElroy, and J. C. G. Walker, "The Diurnal Variation of Ionospheric Temperatures," Planet. Space Sci. 15, 331 (1967)

A. Dalgarno, "Charged Particles in the Upper Atmosphere," Annls. Geophys. 17, 16 (1961)

A. Dalgarno, M. B. McElroy, and R. J. Moffett, "Electron Temperatures in the Ionosphere," Planet. Space Sci., 11, 463 (1963)

A. Dalgarno and T. C. Degges, "Electron Cooling in the Upper Atmosphere," Planet. Space Sci., 16, 125 (1968)

A. Dalgarno, M. B. McElroy and A. I. Stewart, "Electron Impact Excitation of the Dayglow," Journal of the Atmospheric Sciences, 26, 753 (1969)

E. A. Desloge, "Exchange of Energy between Gases at Different Temperatures," Phys. Fluids, 5, 1223 (1962)

REFERENCES CITED
(Continued)

M. J. Druyvesteyn, "Der Niedervoltbogen," Zeit. fur Physik, 64, 790 (1930)

A. G. Englehardt, A. V. Phelps and C. G. Risk, "Determination of Momentum Transfer and Inelastic Collision Cross Sections for Electrons in Nitrogen Using Transport Coefficients," Phys. Rev., 135, 1566 (1964)

A. E. S. Green and C. A. Barth, "Calculation of the Photoelectron Excitation of the Dayglow," J. G. R., 72, 3975 (1967)

R. D. Hake and A. V. Philip, "Momentum-Transfer and Inelastic Collision Cross Sections for Electrons in O_2, CO, and CO_2," Phys. Rev., 158, 70 (1967)

W. B. Hanson, and R. Cohen, "Photoelectron Heating Efficiency in the Ionosphere," J. G. R., 73, 831 (1968)

W. B. Hanson and F. S. Johnson, "Electron Temperatures in the Ionosphere," Memoires Soc. R. Sc. Liege, 4, 390 (1961)

W. B. Hanson, "Electron Temperatures in the Upper Atmosphere," Space Res., 3, 282 (1963)

I. Harris and W. Priester, "Theoretical Models For the Solar-Cycle-Variation of the Upper Atmosphere," Goddard Space Flight Center, (1962)

REFERENCES CITED
(Continued)

K. K. Harris, G. W. Sharp, and W. C. Knudsen, "Ion Temperature and Relative Ion Composition Measurements from a Low-Altitude Polar-Orbiting Satellite," J. G. R., 72, 5939 (1967)

A. E. Hedin and A. O. Nier, "A Determination of the Neutral Composition, Number Density, and Temperature of the Upper Atmosphere from 120 to 200 km with Rocket-borne Mass Spectrometers," J. G. R., 71, 4121 (1966)

A. E. Hedin, D. N. Harpold, J. E. Cooley and C. A. Reker, "Density Fluctuation in the Neutral Atmosphere," A. G. U. Transactions, 51(4), 375 (1970)

W. J. Heikkila and J. D. Winningham, "The Soft Particle Spectrometer," A.G. U. Transaction, 51, 375 (1970)

J. R. Herman and S. Chandra, "The Role of Atomic Oxygen in the Ionosphere E - and F - Region Behavior," Planet, Space Sci., 17, 1247 (1969)

J. R. Herman and S. Chandra, (Private Communications) 1970

REFERENCES CITED
(Continued)

H. E. Hinteregger, "Combined Retarding Potential Analysis of Photoelectrons and Environmental Charged Particles up to 234 km," Space Res., 1, 304 (1960)

H. E. Hinteregger, L. A. Hall, and G. Schmidtke, "Solar XUV Radiation and Neutral Particles Distribution in July 1963 Thermosphere," Space Res., 5, 1175 (1965)

W. R. Hoegy, J. P. Fournier, and E. G. Fontheim, "Photoelectron Energy Distribution in the F Region," J. G. R., 70, 5464 (1965)

P. T. Huang, "Direct Measurements of Electron Energy Distributions in the Daytime Ionosphere," Ph.D. Thesis, University of Maryland, Department of Physics and Astronomy Tech. Rep. No. 936 (1969)

W. C. Knudsen and G. W. Sharp, "Ion Temperatures Measured Around a Dawn-Dusk-Auroral-Zone Satellite Orbit," J. G. R., 72, 1061 (1967)

S. J. Moss and E. Hyman, "Minimum Variance Technique for the Analysis of Ionospheric Data Acquired in Satellite Retarding Potential Analyzer Experiment," J. G. R., 73, 4315 (1968)

H. M. Mott-Smith and I. Langmuir, "Theory of Collectors in Gaseous Discharges," Phys. Rev., 28, 727 (1926)

REFERENCES CITED
(Continued)

A. F. Nagy and J. P. Fournier, "Calculated Zenith Intensity of the Second Positive Bank of Molecular Nitrogen," J. G. R., 70, 5981 (1965)

M. H. Rees, J. C. Walker and A. Dalgarno, "Auroral Excitation of the Forbidden Lines of Atomic Oxygen," Planet. Space Sci., 15, 1097 (1967)

R. C. Sagalyn, M. Smiddy, and J. Wisnia, "Measurement and Interpretation of Ion Density Distribution in the Daytime F Region," J. G. R., 68, 199 (1963)

M. F. Shea, R. D. Sharp, and M. B. McElroy, "Measurements and Interpretation of Low-Energy Photoelectrons," J. G. R., 73, 4199 (1968)

A. K. Sinha, "The Relaxation of Energetic Electrons in Ionospheric Plasma under Wave-Particle Interaction and Coulomb Collision," Ph.D. Thesis, University of Maryland, Department of Physics and Astronomy, To Be Published

K. Smith, R. J. W. Henry and P. G. Burke, "Calculations on the Scattering of Electrons by Atomic Systems with Configurations $2P^q$," Phys. Rev., 157, 51 (1967)

T. Tohmatsu, T. Ogawa and H. Tsuruta, "Photo-Electronic Processes in the Upper Atmosphere, I. Energy Spectrum of the Primary Photo Electrons," Rep. Ion. Space Res. Japan 19, 482 (1965)